Antitoxin autoregulation of *M. tuberculosis* toxin-antitoxin expression through negative cooperativity arising from multiple inverted repeat sequences

Izaak N. Beck[a], Ben Usher[a], Hannah G. Hampton[b], Peter C. Fineran[b], Tim R. Blower[a,*]

[a]Department of Biosciences, Durham University, Stockton Road, Durham, DH1 3LE, UK

[b]Department of Microbiology and Immunology, University of Otago, PO Box 56, Dunedin 9054, New Zealand.

[*]To whom correspondence may be addressed. Email: timothy.blower@durham.ac.uk, tel: +44(0)1913343923.

20

21 # ABSTRACT

22 Toxin-antitoxin systems play key roles in bacterial adaptation, including protection from antibiotic
23 assault and infection by bacteriophages. The type IV toxin-antitoxin system AbiE encodes a DUF1814
24 nucleotidyltransferase-like toxin, and a two-domain antitoxin. In *Streptococcus agalactiae*, the
25 antitoxin AbiEi negatively autoregulates *abiE* expression through positively co-operative binding to
26 inverted repeats within the promoter. The human pathogen *Mycobacterium tuberculosis* encodes
27 four DUF1814 putative toxins, two of which have antitoxins homologous to AbiEi. One such *M.*
28 *tuberculosis* antitoxin, named Rv2827c, is required for growth and whilst the structure has
29 previously been solved, the mode of regulation is unknown. To complete the gaps in our
30 understanding, we first solved the structure of *S. agalactiae* AbiEi to 1.83 Å resolution for
31 comparison with *M. tuberculosis* Rv2827c. AbiEi contains an N-terminal DNA binding domain and C-
32 terminal antitoxicity domain, with bilateral faces of opposing charge. The overall AbiEi fold is similar
33 to Rv2827c, though smaller, and with a 65° difference in C-terminal domain orientation. We further
34 demonstrate that, like AbiEi, Rv2827c can autoregulate toxin-antitoxin operon expression. In
35 contrast to AbiEi, the $P_{rv2827c}$ promoter contains two sets of inverted repeats, which bind Rv2827c
36 with differing affinities depending on the sequence consensus. Surprisingly, Rv2827c bound with
37 negative co-operativity to the full $P_{rv2827c}$ promoter, demonstrating an unexpectedly complex form of
38 transcriptional regulation.

39

40

41 # KEYWORDS

42 Toxin-antitoxin systems, negative co-operativity, *Mycobacterium tuberculosis*, abortive infection,
43 AbiE

44

45 # INTRODUCTION

46 Toxin-antitoxin (TA) systems are encoded by genetic loci that are widely distributed throughout
47 prokaryotic genomes. They can play pivotal roles in bacterial physiology and in managing stress
48 responses, helping bacteria to survive nutrient limitation, immune system attack, antibiotic
49 treatment and predation by bacteriophages [1–5]. TA systems are commonly found on mobile
50 genetic elements, contributing to the stability of plasmids, superintegrons, cryptic prophages and
51 conjugative transposons [6–8]. The majority of TA systems encode two components, a toxic protein
52 that generally targets essential cellular processes, and an antagonistic antitoxin [4]. This antitoxin
53 negates toxin activity when cells are growing in favorable conditions. Under stressful conditions, the
54 antitoxin is preferentially degraded and the toxin is released, thereby reducing growth rate as a
55 means to survive with minimal metabolic burden until favorable conditions return [9,10]. Activation
56 of the toxin following bacteriophage infection can also lead to the removal of the infectious
57 bacteriophage particle from the environment, thereby providing a population level protection from
58 viruses referred to as abortive infection (Abi) [11,12].

59

60 TA systems have been divided into six types according to the nature of the toxin and antitoxin
61 (whether they are RNA or protein), and the mechanism of toxin antagonism [4]. Type IV systems
62 differ from all others in that the antitoxin and toxin do not directly interact, instead, the antitoxin
63 antagonises the activity of the toxin [13–15]. There are multiple examples wherein TA systems
64 provide a phage-resistant Abi phenotype, although not all identified Abi systems act as *bona fide* TA
65 systems [5,15–20]. A recently characterised Abi system, AbiE from *Streptococcus agalactiae* V/R
66 2603, has been shown to act as a type IV TA system [15]. AbiE encodes a DUF1814-family toxin
67 (AbiEii), and a COG5340-family antitoxin (AbiEi) (**Fig. 1A**) [15]. The *S. agalactiae* AbiE COG5340
68 antitoxin will herein be referred to as AbiEi. AbiEii is a putative nucleotidyltransferase (NTase) that

69 specifically binds GTP [15]. This DUF1814 family is widespread, present in over 5,500 bacterial,
70 archaeal and fungal genomes, though not all examples are genetically linked to putative antitoxins.

71

72 TA systems are remarkably abundant in *Mycobacterium tuberculosis*, which encodes more than 80
73 examples, and these are thought to have contributed to *M. tuberculosis* having become the most
74 successful human pathogen [21–24]. *M. tuberculosis* H37Rv encodes four DUF1814-family NTase-like
75 putative toxins, namely Rv0078A, Rv0836c, Rv1045 and Rv2826c (**Fig. 1A**). Akin to AbiEii from *S.*
76 *agalactiae*, both Rv1045 and Rv2826c have a cognate COG5340-family antitoxin (**Fig. 1A**).
77 Transposon mutagenesis studies have identified the cognate antitoxins of these systems (Rv1044
78 and Rv2827c) as essential for lab growth [25,26], suggesting that Rv1045 and Rv2826c toxins are
79 functional in *M. tuberculosis*. The *M. tuberculosis* COG5340 proteins will herein be referred to by
80 their respective 'Rv' identifiers, Rv1044 and Rv2827c. Characterizing and understanding the
81 regulation of these loci is of interest for developing new therapies against the pathogen.

82

83 Autoregulation of TA system expression is a hallmark of type II TA systems and can be either positive
84 or negative [27,28]. The antitoxin AbiEi from *S. agalactiae* has been biochemically characterized
85 [15,29] and functions as both an antitoxin and a transcriptional repressor. That is, AbiEi negatively
86 autoregulates *abiE* expression. Here, the gene product suppresses its own production, through
87 positively co-operative binding of two AbiEi monomers to inverted repeats in the promoter region.
88 Full length AbiEi is required for negative autoregulation and induced bending of the promoter DNA.
89 We previously proposed that this bending was facilitated by the two AbiEi monomers interacting via
90 their C-terminal domains (CTDs) [29]. In contrast to type II autoregulation, for which conditional co-
91 operativity is observed, co-expression of the cognate toxin AbiEii does not enhance transcriptional
92 repression [15]. We therefore sought to determine the similarities in the structure and function of

93 AbiEi and Rv2827c. While the structure of the *M. tuberculosis* putative antitoxin Rv2827c has been
94 solved as part of a structural genomics initiative [30], its biological function was not explored and it
95 has not been biochemically characterized. We present the solved structure of *S. agalactiae* AbiEi,
96 demonstrating structural homology between the COG5340 antitoxins, and biochemically
97 characterize the molecular interactions underpinning transcriptional repression by Rv2827c.
98 Interestingly, this is a more complex autoregulatory system than previously seen for AbiEi [29].

99

100

101

102

103

104

105

106

107

108

109

110

111

112

113 # MATERIALS AND METHODS

114 ## Bacterial strains and culture conditions

115 *E. coli* DH5α (Invitrogen), BL21 (DE3) (Invitrogen) and ER2566 (New England Biolabs) were routinely
116 grown at 37 °C in Luria-Broth (LB), M9 minimal (M9M), or 2x YT media supplemented when
117 necessary with ampicillin (Ap, 50 μg/ml), spectinomycin (Sp, 100 μg/ml), tetracycline (Tc, 10 μg/ml),
118 isopropyl-β-D-thiogalactopyranoside (IPTG, 1 mM), L-arabinose (L-ara, 0.1% w/v) or D-glucose (glu,
119 0.2% w/v). Bacterial cell density was measured using a WPA Biowave C08000 at 600 nm (OD_{600}).

120

121 ## DNA isolation and manipulation

122 All oligonucleotides used in this study were obtained from Integrated DNA Technologies (**Table S1**).
123 Plasmid and PCR-amplified DNAs were purified using Monarch kits (NEB). Digests, ligations,
124 transformations and agarose gel electrophoresis steps were performed by standard techniques. All
125 constructed plasmids (**Table S2**) were confirmed by sequencing using an ABI 3730 DNA sequencer
126 and 4Peaks.

127

128 Protein expression constructs were made by Ligation Independent Cloning (LIC) [31]. Target genes
129 were cloned into plasmid pSAT1-LIC, which generates N-terminal His_6-SUMO fusions with the target
130 ORF. Primers TRB1048/TRB1049 were used to amplify *abiEi* from pRLD30, for LIC insertion into
131 pSAT1-LIC, producing pTRB525. Primers TRB1022/TRB1023 were used to amplify *rv2827c* from
132 pPF658, also for LIC insertion into pSAT1-LIC, producing pTRB493. Primers TRB1018/TRB1019 were
133 used to amplify *rv1044* from *M. tuberculosis* H37Rv genomic DNA (ATCC), again for LIC insertion into
134 pSAT1-LIC, producing pTRB491.

135

136 For promoter activity assays, regions upstream of *abiEi*, *rv2827c* and *rv1044* were cloned into
137 pRW50 [32]. The 99 bp region upstream of *abiEi* was amplified from pPF680 using primers
138 TRB1072/TRB1047, then digested with EcoRI/HindIII and ligated into pRW50 cut with the same
139 enzymes, producing pTRB486. The 500 bp regions upstream of *rv2827c* and *rv1044* were amplified
140 from H37Rv genomic DNA, using primers TRB1042/TRB1043 and TRB1040/TRB1041, respectively.
141 The amplicons were digested with EcoRI/HindIII and ligated into pRW50 cut with the same enzymes,
142 producing pTRB484 and pTRB483, respectively. Antitoxin genes *abiEi, rv2827c and rv1044* were
143 cloned into pTA100, a pQE-80 derivative [5]. *S. agalactiae abiEi* was amplified from pRLD30 using
144 primers TRB1052/TRB1053 the digested with EcoRI/HindIII and ligated into pTA100 cut with the
145 same enzymes, producing pTRB481. *M. tuberculosis rv2827c* and *rv1044* were amplified from H37Rv
146 genomic DNA, using primers PF1334/PF1335 and PF1330/PF1331 respectively. The amplicons were
147 digested with NdeI/SpeI and ligated into pTA100 cut with the same enzymes, producing pPF658 and
148 pPF658, respectively.

149

150 Protein expression and purification

151 To express AbiEi, Rv2827c and Rv1044 for crystallization and/or biochemistry, *E. coli* ER2566 (for
152 native protein) or BL21 (DE3) (for labelled protein) were transformed with pTRB525, pTRB493 or
153 pTRB491, respectively. For native protein, overnight cultures were re-seeded 1:100 into 2 L flasks
154 containing 1 L 2x YT. Cells were grown at 150 rpm in 37 °C until an OD_{600} of 0.6-0.8 was reached,
155 whereupon expression was induced by the addition of IPTG (1 mM). Cells were left to grow for 16 h
156 at 17 °C, shaking at 150 rpm.

157

158 For incorporation of selenomethionine into AbiEi, the SeMet kit (Molecular Dimensions) was used.
159 Starter cultures of BL21 (DE3) pTRB525, starter cultures were grown for 8 hours in LB at 37 °C with
160 200 rpm shaking. This culture was used to inoculate (1:500) a 50 mL overnight of Molecular
161 Dimensions Selenomethionine Base medium supplemented with Molecular Dimensions Nutrient
162 Mix. This overnight was then used to inoculate (1:100) 1 L of the same Base Medium with Nutrient
163 Mix and cells were grown at 37 °C with 180 rpm shaking. At OD_{600} 0.8 cells were pelleted by
164 centrifugation at 4200 x g, resuspended in fresh Base Medium with Nutrient Mix (Molecular
165 Dimensions) and supplemented with an amino acid mix to promote feedback inhibition of
166 methionine synthesis (0.1 mg/ml L-lysine hydrate, 0.1 mg/ml L-threonine, 0.1 mg/ml L-
167 phenylalanine, 0.05 mg/ml L-leucine, 0.05 mg/ml L-isoleucine, 0.05 mg/ml L-valine). Cells were
168 grown for a further 30 minutes at 37 °C with shaking at 180 rpm before the addition of 250x
169 SelenoMethionine Solution (Molecular Dimensions) to a final concentration of 40 µg/mL. Cells were
170 grown for a further 15 minutes at 37 °C with shaking at 180 rpm before antitoxin expression was
171 induced with IPTG (1 mM), and samples were left to grow overnight at 175 rpm in 18 °C.

172

173 For native protein purification, bacteria were harvested by centrifugation at 4200 x g and the pellets
174 were resuspended in buffer A500 (20 mM Tris-HCl pH 7.9, 500 mM NaCl, 5 mM imidazole and 10%
175 glycerol). Cells were lysed by sonication at 40 kpsi, then centrifuged (45,000 x g, 4 °C). The clarified
176 lysate was next passed over a HisTrap HP column (GE Healthcare), washed for ten column volumes
177 with A500, followed by ten column volumes of buffer A100 (20 mM Tris-HCl pH 7.9, 100 mM NaCl, 5
178 mM imidazole and 10% w/v glycerol), then eluted directly onto a HiTrap Q HP column (GE
179 Healthcare) with buffer B100 (20 mM Tris-HCl pH 7.9, 100 mM NaCl, 250 mM imidazole and 10% w/v
180 glycerol). The Q HP column was transferred to an Äkta Pure (GE Healthcare), washed with three
181 column volumes of A100, then proteins were eluted using a gradient from 100% A100 to 100%
182 buffer C1000 (20 mM Tris-HCl pH 7.9, 1000 mM NaCl and 10% w/v glycerol). Fractions containing the

183 protein peak were analysed by SDS-PAGE, pooled and incubated overnight at 4 °C with hSENP2
184 SUMO protease to cleave the His_6-SUMO tag from the target protein. The following day, the samples
185 were passed through a second HisTrap HP column and the flow-through fractions containing
186 untagged target protein were collected. The same procedure was used for labelled protein, except
187 seleno-AbiEi precipitated on column at A100, contaminants were removed with B100, and remaining
188 folded seleno-AbiEi was eluted with B500, followed by SENP cleavage and a second HisTrap column
189 purification. Proteins were dialysed overnight at 4 °C into buffer X (20 mM Tris-HCl pH 7.9, 200 mM
190 NaCl and 2.5 mM DTT). Crystallization samples were concentrated, quantified and stored on ice,
191 then either used immediately or flash-frozen in liquid N_2 for storage at -80 °C.

192

193 **Protein crystallization**

194 Native and selenomethionine-derivatized AbiEi were concentrated to 12 mg/ml in buffer X (see
195 above). Initial native AbiEi crystallization screens were performed using commercial screens
196 (Molecular Dimensions) set with an Innovadyne Screenmaker robot, making 200:100 nl and 100:100
197 nl protein:condition sitting drops at 18 ^{o}C. After initial screening and optimization, native AbiEi
198 formed thick needles in 0.02 M Sodium/Potassium phosphate, 0.1 M Bis-Tris Propane pH 6.5, 20%
199 PEG 3350. Selenomethionine-derivatized AbiEi crystals grew in 0.2 M Sodium acetate trihydrate, 0.1
200 M Bis-Tris Propane pH 6.5, 15% PEG 3350. To harvest, 20 µl of condition reservoir was added to 20 µl
201 of glycerol and mixed quickly by vortexing; an equal volume of this mixture was then added to the
202 drop volume. After addition of cryo buffer, crystals were immediately extracted using a nylon loop
203 and flash-frozen in liquid N_2.

204

205 **X-ray data collection and structure determination**

206 Diffraction data were collected at Diamond Light Source on beamlines I03 (AbiEi native) and I03
207 (AbiEi selenomethionine-derivatized) (Table 1). Single, 360°, datasets were collected from three
208 native AbiEi crystals and merged using iSpyB (Diamond Light Source). Two, 360°, datasets from AbiEi
209 selenomethionine-derivatized crystals measured at the selenium peak (0.9793 Å) were also merged
210 using iSpyB. An additional AbiEi selenomethionine-derivatized dataset was collected at selenium
211 high remote (0.9641 Å) wavelength. Diffraction data were processed with XDS [33,34], and then
212 AIMLESS from CCP4 [35] was used to corroborate the spacegroups (Table 1). The crystal structure of
213 AbiEi was solved by MAD, by providing the SHELX suite [36] in CCP4 with the native, peak and high
214 remote datasets. The solved starting model for AbiEi was built in REFMAC [37] and BUCCANEER [38].
215 The model was then iteratively refined and built using PHENIX [39] and COOT [40], respectively. The
216 quality of the final model was assessed using COOT and the wwPDB validation server [41]. Structural
217 figures were generated using PyMol (Schrödinger). Structural alignments were performed using
218 PROMALS3D [42].

219

220 Electrophoretic Mobility Shift Assays

221 Conservation of IR sequences was determined using MView [43] and WebLogo [44]. Promoter region
222 probes were amplified from synthesised templates (Table S1). Each template was made with a
223 common downstream region, matching the initial part of *lacZ* from pRW50. For each probe
224 template, a unique upstream forward primer was used in combination with a common reverse
225 primer, which was either untagged or had been conjugated to a fluorescein tag for visualization
226 (Table S1). The probes contained either the native promoter regions, or combinations of WT IR
227 sequences and mutant sequences of polyC.

228

229 Proteins were diluted to appropriate concentrations using diluent buffers matching their storage
230 buffer constitution. Each binding reaction contained 2 µL of 5x EMSA binding buffer (750 mM KCl, 50
231 mM Tris-HCl pH 8.0, 2.5 mM EDTA pH 8.0, 0.5 % Triton X-100, 1 mM DTT, 55% glycerol), 250 fmoles
232 of fluorescently labelled probe, 0.1 µL BSA (10 mg/ml), 1 µL poly(d[IC]) (1 mg/mL), 1 µL of diluted
233 protein or buffer control and water to a final volume of 10 µL. Native 0.5x TBE polyacrylamide gels
234 (at either 7% or 5% acrylamide, as required) were pre-run at 150 V and 4 ^{o}C for 2 h. Binding reactions
235 were titrated at protein concentrations from zero to an appropriate upper limit, and incubated at 20
236 ^{o}C for 30 min. Non-specific binding controls used an additional excess of 2.5 µM TRB1108 template
237 DNA amplified with TRB1109 as forward primer, and non-labelled reverse primer. Specific binding
238 controls used additional excess of 2.5 µM unlabelled specific probe DNA. Samples were then
239 separated by native polyacrylamide gel electrophoresis at 200 V and 4 ^{o}C for 45 min.

240

241 Native polyacrylamide gels were then visualised using the Amersham Biosciences Typhoon 9400 on
242 variable mode image in fluorescence mode, emission filter 526 SP. Sensitivity was set to normal.
243 Band intensities were calculated using the grid scan feature and triplicate data processed in Prism
244 (GraphPad Software). Fractional saturation curves were produced with fractional saturation, Y,
245 varying from 0 – 1.0. Y values are calculated by (Y/(Y+(1-Y))) and plotted against protein
246 concentration. Data were converted to the Hill plot to analyse the degree of cooperativity in the
247 binding events, characterised by the Hill coefficient (slope of the plot at log(θ)=0). The Hill plot is
248 constructed by plotting logθ against log[protein], with θ defined as (θ = (Y/(1-Y))). Dissociation
249 coefficients (Kd) can also be extracted from the Hill plot as Kd = $10^{X\text{-intercept}}$. Mean and standard error
250 of the mean values are derived from at least three independent experiments.

251

252 **Promoter activity assays**

253 Promoter regions were cloned into the promoterless *lacZ* fusion plasmid, pRW50 [32]. Antitoxin
254 genes were cloned into the pQE-80 derivative, pTA100 [5] for tight control of antitoxin expression.
255 Construction is detailed above. Promoter activity assays were performed as described previously
256 [45,46]. Briefly, *E. coli* DH5α were co-transformed with the *lacZ* reporter constructs pTRB483 (P_{rv1044}),
257 pTRB484 ($P_{rv2827c}$) or pTRB486 (P_{abiEi}), and the IPTG-inducible pTA100-antitoxin plasmids pPF656
258 (Rv1044), pPF658 (Rv2827c) or pTRB481 (AbiEi). Transformants were re-seeded from overnight
259 cultures and grown in 37 °C at 200 rpm in LB supplemented with Tc, Sp, and with/without IPTG until
260 mid-log phase, then 80 µl of cells were added to 120 µl master mix (60 mM Na_2HPO_4, 40 mM
261 NaH_2PO_4, 10 mM KCl, 1 mM $MgSO_4$, 36 mM β-mercaptoethanol, 166 µl/ml T7 lysozyme, 1.1 mg/ml
262 ONPG, and 6.7 % PopCulture Reagent (Merck Millipore)) in corresponding wells of a 96-well plate.
263 This was then placed in a SPECTROstar Nano absorbance plate reader (BMG LABTECH) set to 30 °C
264 with shaking at 500 rpm, wherein OD_{600} and OD_{420} readings were taken every 90 seconds for 1 hour.
265 Data analysis was performed in the MARS Data Analysis software package (BMG LABTECH). The
266 kinetic OD_{420} readings were converted into the slope of OD_{420} over time (OD_{420}/min). These values
267 were multiplied by 5000 and divided by the OD_{600} reading from the first time point to generate
268 Miller Units (mU). Plotted data are the normalized mean and standard deviation obtained from
269 three independent experiments.
270

271

272 ## Accession number

273 The crystal structure of AbiEi has been deposited in the Protein Data Bank under accession number
274 6Y8Q.

275

276 # RESULTS

277 ## AbiEi-family antitoxins contain conserved structural features

278 We had previously hypothesized that there was structural similarity between the biochemically
279 characterised antitoxin AbiEi from *S. agalactiae* [29] and the structurally characterised homologue,
280 Rv2827c [30]. We sought to confirm structural and biochemical similarity between these two
281 proteins, and within the broader COG5340 antitoxins. To begin, we solved a 1.83 Å structure of AbiEi
282 by X-ray crystallography (**Figs. 1B and C, Table 1**). There were four copies of AbiEi in the asymmetric
283 unit, forming minor crystal contacts that are not predicted to be biologically relevant, and each copy
284 contains minor variations in domain orientation, indicating some flexibility. Together with previous
285 size exclusion chromatography data [29], we concluded that AbiEi is a 23 kDa monomer in solution.

286

287 AbiEi contains an N-terminal winged helix-turn-helix DNA-binding domain and a C-terminal antitoxin
288 domain, connected by a short linker (**Fig. 1B**). Mutagenesis studies have demonstrated that full-
289 length AbiEi is required for negative autoregulation of the P_{abiE} promoter, whilst the C-terminal
290 domain alone is sufficient for antitoxicity against the effects of AbiEii [15]. The N-terminal domain
291 contains three α-helices, followed by three beta-strands forming an antiparallel sheet (**Fig. 1B**). The
292 C-terminal domain begins with a single α-helix that is separated from a six-helix bundle by a row of
293 four β-strands, which themselves pair into parallel and antiparallel β-sheets (**Fig. 1B**). One face of
294 AbiEi is positively charged, and the reverse face is negatively charged (**Fig. 1C**). The positive side
295 corresponds with the site of positively charged sidechains distributed throughout the N-terminal and
296 C-terminal domains, which have previously been shown to be vital for DNA-binding and
297 autoregulation through mutagenesis studies [29]. When AbiEi is compared with Rv2827c, both are
298 monomers and it is clear that the two antitoxins share the two-domain structure and charge
299 features (**Figs. 1B-E**).

300

301 When AbiEi and Rv2827c are aligned via the N-terminal winged helix-turn-helix domain, the
302 respective C-terminal domains differ in position relative to the N-terminal domains by approximately
303 65° (**Fig. 2A**). We propose that these different poses captured in the crystal structures might reflect
304 variable positions of the C-terminal domains potentially allowed by a linker joining the two domains.
305 The stability of the B-factors for the subdomains AbiEi and Rv2827c, alongside lack of significant
306 variation in the domain orientations within the asymmetric unit indicates a preferred state has been
307 captured in the crystal. This however would require further analysis in solution. The extensive
308 nature of the AbiEi charged surface, the requirement for the full AbiEi protein for autoregulation
309 [15], and the presence of a flexible linker altogether indicate the full protein is needed for DNA
310 interactions and DNA bending as per our previously proposed model [29].

311

312 When the N-terminal domain helices and C-terminal domains from AbiEi and Rv2827c are separated
313 and structurally superposed, it is possible to see an approximate overlay between corresponding
314 regions, with RMSDs of 3.04 Å for the N-terminal helices and 3.41 Å for the C-terminal domains (**Fig.**
315 **2B and C**). The N-terminal domains have conserved positioning of key helices H2 and H3, which are
316 used within winged helix-turn-helix domains for stabilization and DNA recognition, respectively [47]
317 (**Fig. 2B**). The C-terminal domain of AbiEi is the smaller of the two; performing a structure-based
318 sequence alignment of AbiEi and Rv2827c shows that Rv2827c has an extended C-terminal domain
319 55 amino acids longer than AbiEi (**Fig. S1**). Despite this extension, AbiEi and Rv2827c share a
320 conserved common core fold of unknown function (**Fig. 2C**). When AbiEi was compared against the
321 PDB to look for similar structures, using the DALI server [48], Rv2827c was the top hit followed by
322 bacterial antibiotic-modifying adenylyltransferases (PDB codes 5KQJ, 4FO1), and a putative fungal
323 NTase (PDB: 5UVD). These putative biochemical activities for AbiEi match well with the NTase

324 activity of the cognate toxin AbiEii [15]. Overall, despite differing captured poses and discrepancy in
325 size, AbiEi and Rv2827c are markedly similar in domain structure, fold and surface charge and are
326 therefore structural homologues.

327

328 It has been shown that the AbiEi C-terminal domain is required for negative autoregulation and likely
329 contributes to positive cooperativity through C-terminal domain interactions [29]. The cons-PPISP
330 server [49] was used to highlight the residues most likely to be critical for protein-protein
331 interactions for both AbiEi and Rv2827c (**Fig. 2D-E**). In the AbiEi monomer, 16 identified residues
332 were clustered at the C-terminus, forming a putative site for interaction (**Fig. 2D**). For Rv2827c,
333 however, the diffuse scattering of 34 identified residues along the structure (**Fig. 2E**) predicts that
334 there may be no obvious interface for protein-protein interactions. This is reinforced by the different
335 positioning of the CTD seen in Rv2827c (**Fig 2A**). These findings suggest that the interactions of AbiEi
336 C-terminal domains could contribute to positive co-operativity in promoter binding, supporting our
337 previously proposed model, whereas for Rv2827c, such interactions are unlikely to occur and
338 indicate a different mechanism of DNA-binding and autoregulation.

339

340 Rv2827c binds two sets of inverted repeats

341 AbiEi binds to two 23 bp inverted repeats (IR1 and IR2) within the promoter of P_{abiEi}, which are
342 separated by 3 bp [29] (**Fig. 3A**). Examination of the upstream region of $P_{rv2827c}$ revealed two pairs of
343 23 bp inverted repeats within the region -1 to -131 bp from the *rv2827c* start codon, that also
344 overlap the promoter (**Fig. 3A**). These four repeats (IR1 to IR4) are arranged in tandem with a 4 bp
345 gap between the two pairs of inverted repeats and a 13 bp gap between the repeats within each pair
346 (**Fig. 3A**). As P_{abiEi} repeats are separated by 3 bp and the repeats within pairs from $P_{rv2827c}$ are
347 separated by 13 bp, it is possible the additional 10 bp accommodates binding of the larger C-

348 terminal domains of Rv2827c (**Fig. S1**). Using the bacterial promoter prediction software
349 CNNPromoter_b [50], the IR3-IR4 repeats were predicted to straddle a binding site for the primary
350 *M. tuberculosis* sigma factor SigA [51]. As Rv2827c binding would sterically hinder sigma factor
351 binding, in turn, this would prevent transcription of the operon by RNA polymerase. When IR1-IR4
352 sequences from $P_{rv2827c}$ were aligned with IR1-IR2 sequences from P_{abiEi}, the sequence similarity
353 indicated possible conservation of binding sequence (**Fig. 3B**). We therefore hypothesized that
354 despite sharing low protein sequence identity (17.7%), Rv2827c might bind these $P_{rv2827c}$ inverted
355 repeats similarly to AbiEi binding its cognate P_{abiEi} repeats.

356

357 The four $P_{rv2827c}$ 23 bp inverted repeats were first tested as two consecutive pairs, to allow a direct
358 comparison to the arrangement of P_{abiEi} [29]. Analysis began with IR3-IR4, the pair overlapping the
359 transcriptional start and therefore analogous to IR1-IR2 of P_{abiEi} (**Fig. 4A**). Using electrophoretic
360 mobility shift assays (EMSAs), Rv2827c was shown to bind both of the IR3-IR4 inverted repeats
361 within the -1 to -71 region (**Fig. 4B**). Sequential removal of the inverted repeats by mutating one, the
362 other or both to poly-C tracts reduced Rv2827c-DNA interaction to a single binding event (**Fig. 4C**
363 **and D**) or ablated binding completely (**Fig. 4E**). Analysis of IR3-IR4 binding (**Fig. 4B and F**) showed
364 weak saturation of binding. The calculated Hill co-efficient indicates that IR3-IR4 binding by Rv2827c
365 is not co-operative (**Fig. 4G**).

366

367 Similar results were obtained when testing the IR1-IR2 repeats within the -61 to -131 region of
368 $P_{rv2827c}$ (**Fig. 5A-G**). In this case, there was greater saturation of binding to IR1-IR2 (**Fig. 5F**) than to
369 IR3-IR4 (**Fig. 4F**). The Hill co-efficient surprisingly indicated weakly negative co-operativity in Rv2827c
370 binding to IR1 and IR2 (**Fig. 5G**), in comparison to the non-co-operative binding observed with IR3
371 and IR4 (**Fig. 4G**). To allow direct comparison between model systems, we also performed the same

372 assays with purified AbiEi and probes for P_{abiEi} (**Fig. S2**). This corroborated previous data [29] and
373 under our experimental conditions, AbiEi bound more tightly to its cognate inverted repeats (**Fig.**
374 **S2F**), than either Rv2827c binding to IR3-IR4 (**Fig. 4F**) or IR1-IR2 (**Fig. 5F**), and also demonstrated
375 clear positive co-operativity (**Fig. S2G**).

376

377 Due to similarity of structure, functionality and cognate DNA inverted repeat sequences, we
378 hypothesized that AbiEi and Rv2827c might bind their respective non-cognate promoter regions.
379 However, AbiEi did not bind either pair of inverted repeats from $P_{rv2827c}$ (**Fig. S3A and B**). Similarly,
380 Rv2827c did not bind IR1-IR2 of P_{abiEi} (**Fig. S3C**).

381

382 Rv2827c binds with negative co-operativity

383 Having investigated the two sets of $P_{rv2827c}$ inverted repeats independently, a full-length probe
384 covering the $P_{rv2827c}$ region -1 to -131 was generated to examine the interaction of Rv2827c protein
385 with all four inverted repeats. Using EMSAs, four distinct protein-bound DNA species were observed,
386 indicating that all four inverted repeats can be bound simultaneously by Rv2827c (**Fig. 6A**). The four
387 binding sites did not fully saturate (**Fig. 6B**), and the Hill coefficient confirmed negatively co-
388 operative binding of Rv2827c across these four inverted repeats (**Fig. 6C**). Displaying the saturation
389 curve data on a semi-log scale highlights breaks and multiple distinct gradients in the binding curve,
390 eluding to multiple individual binding events (**Fig. 6D**). Negatively co-operative binding by Rv2827c
391 to $P_{rv2827c}$ contrasts with the positive co-operativity observed for AbiEi binding to P_{abiEi} [29].

392

393 Our earlier data using mutant probes provided insight into how Rv2827c binds to individual repeats
394 (**Fig. 4C and D, Fig. 5C and D**). These were used to calculate the binding affinity of Rv2827c for each

395 individual IR sequence, with IR1 most tightly bound (K_d of 0.0205 µM), closely followed by IR4 (K_d of
396 0.121 µM), then IR2 (K_d of 0.862 µM), and finally IR3 (K_d of 11.0 µM) (**Fig. 6E-M**). This descending
397 affinity series creates a wide range of concentrations across which negative autoregulation by
398 Rv2827c can occur. These data demonstrate the same core principles of promoter binding are used
399 by both AbiEi and Rv2827c, but that these have been employed evolutionarily for differing modes of
400 regulation.

401

402 Rv1044 is a DNA-binding protein, but fails to recognize the cognate
403 promoter

404 Whilst it had not been possible to identify inverted repeats within the *rv1044-rv1045* locus, two,
405 slightly overlapping, 70 bp probes were generated to cover the 131 bp region upstream of the
406 *rv1044* translational start site, and used to test Rv1044 binding (**Fig. S4A and B**). No binding event
407 was observed with either probe (**Fig. S4A and B**). Nevertheless, we wanted to test whether Rv1044
408 was competent for DNA-binding and so cross-reacted Rv1044 with the two probes covering IR3-IR4
409 and IR1-IR2 of $P_{rv2827c}$, and the probe containing IR1-IR2 of P_{abiEi} (**Fig. S4C, D and E**). No binding was
410 observed for either of the $P_{rv2827c}$ probes (**Fig. S4C and D**), but curiously, Rv1044 bound the inverted
411 repeats of P_{abiEi} (**Fig. S4E**). Rv1044 bound more weakly than AbiEi to P_{abiEi} IR1-IR2 (**Fig. S4F**), and
412 showed no co-operativity (**Fig. S4G**). This demonstrates that Rv1044 can bind DNA in a sequence-
413 specific manner, and so we looked for potential targets in the *M. tuberculosis* H37Rv genome. The
414 *abiE* IR sequences align with numerous positions in the *M. tuberculosis* genome but not upstream of
415 any of the DUF1814 TA systems. This may indicate a potential role for Rv1044 in regulating genes
416 outside of the *rv1044-rv1045* operon, as has been shown in other TA systems whereby antitoxins
417 influence gene expression in biofilm formation pathways [52–54]. A further study will be needed to
418 fully explore any potential regulatory role of Rv1044.

419

420 ## Rv2827c negatively autoregulates Rv2827c-Rv2826c expression

421 Having shown a structural similarity between the two antitoxins, we next sought to test whether the
422 COG5340 proteins from *M. tuberculosis* could function as autoregulators, like characterized AbiEi
423 [29]. AbiEi negatively autoregulates expression from the P_{abiEi} promoter [29]. To examine whether
424 Rv2827c and also the second *M. tuberculosis* COG5340 protein, Rv1044, also perform negative
425 autoregulation, we first cloned the 500 bp region upstream of each respective translational start site
426 into a promoterless *lacZ*-reporter plasmid [32]. For comparison, the equivalent P_{abiEi}–reporter,
427 containing the previously identified promoter region identified in the upstream 99 bp [15,29] was
428 also tested. Both P_{abiEi} and $P_{rv2827c}$ reporters yielded expression of LacZ, but P_{rv1044} did not (**Fig. 7A**).
429 The two active reporter constructs P_{abiEi} and $P_{rv2827c}$, were then paired with inducible plasmids for
430 expression of the cognate antitoxins, and LacZ levels were determined with and without antitoxin
431 induction (**Fig. 7B**). When compared to the uninduced controls, both antitoxins negatively
432 autoregulated expression from their cognate promoters (**Fig. 7B**) demonstrating that Rv2827c and
433 AbiEi share not only a common structure, but also a common negative autoregulatory function.

434

435 # DISCUSSION

436 In this study we present the crystal structure of *S. agalactiae* AbiEi, which was the first type IV TA
437 system antitoxin shown to be capable of transcriptional autoregulation through promoter binding
438 [29]. Further to this, we have demonstrated the autoregulatory capacity of the related Rv2827c
439 antitoxin, a protein of known structure [30]. Whilst AbiEi is a structural homologue of the Rv2827c
440 antitoxin, and both share similar promoter architectures, they have distinct differences in their size
441 and captured domain orientations. We also show that negative autoregulation of the $P_{rv2827c}$
442 promoter operates via negatively co-operative interactions.

443

444 Despite the low shared sequence similarity seen for the COG5349 antitoxins investigated (AbiEi and
445 Rv2827c – 17.7 %; AbiEi and Rv1044 – 21.2 %; Rv2827c and Rv1044 – 24.5 %), we have
446 demonstrated structural conservation across species. As sequences diverge, structure is conserved
447 (**Fig. 1, Fig. 2**), which maintains the shared functionality of these antitoxins, for instance, DNA-
448 binding (**Figs. 4–7, Figs. S2–S4**). Interestingly, sequence variation of the NTD, alongside differing
449 promoter architectures, has resulted in at least three variations of antitoxicity. AbiEi and Rv2827c
450 both autoregulate their own operons, albeit with contrasting types of cooperativity. Rv1044,
451 however, may regulate genes elsewhere in the *M. tuberculosis* genome, given the lack of affinity to
452 the *rv1044* upstream region tested (**Fig. S4A-B**) and absence of identifiable inverted repeats, but
453 apparent DNA-binding capabilities (**Fig. S4E-G**). Further analysis will be required to identify a
454 functional promoter for the *rv1044-rv1045* operon and confirm any potential regulatory function of
455 Rv1044. The antitoxic CTDs have a common core fold that are predicted to have NTase activity based
456 on structure-based functional searches [30]. Therefore, the antitoxic mechanism is likely conserved,
457 despite low sequence similarity within these domains (**Fig. S1**). As protein sequences will be tuned to
458 the needs of the organism, we have shown a correspondingly differential pattern of residues for

459 protein-protein interactions (**Fig. 2D-E**) which, alongside the different CTD positions captured (**Fig.**
460 **2A),** may contribute to individual autoregulation requirements. Our previous model predicted AbiEi
461 C-terminal domain interactions promote positive co-operative binding and result in DNA-bending
462 [29], however this does not appear to apply to Rv2827c. Our proposed model (**Fig. 8**) implies a
463 possible lack of protein-protein interactions supported by predicted interaction interfaces (**Fig. 2D-**
464 **E**), while not ruling out the potential for steric restriction. Rather, promoter inverted repeat
465 sequence 'tuning' (**Fig. 3**) contributes to the negatively co-operative interaction via descending
466 affinities.

467

468 Promoters of *M. tuberculosis* are known to be more complex than those of *E. coli*; they can stretch
469 to 2000 bp from the start site and lack canonical elements such as the conserved -35 sequence [55–
470 57]. Transcriptional regulation is complicated further when considering the vast number of sigma
471 factors [58] and environmentally responsive transcription factors [59] present in *M. tuberculosis*,
472 allowing for greater promoter sequence variation. The -10 sequence for *rv2827c-rv2826c* is a
473 predicted recognition site for principle *M. tuberculosis* sigma factor SigA, which is usually maintained
474 at a constant level for cellular "housekeeping" [51]. SigA also has a role in host-pathogen
475 interactions, controlling growth rates during macrophage infection [60] and regulating virulence
476 genes through both constitutive and upregulated expression [61–63]. Deletions of *rv2827c* cause a
477 growth defect [25,26], suggesting SigA drives expression and that there is potential for output to be
478 tuned by SigA and Rv2827c levels according to environmental cues. Previous reports on the type IV
479 antitoxin CbeA demonstrate a positive effect on cytoskeletal bundling alongside antitoxicity and the
480 ability to counteract chemical inhibitors of cytoskeletal polymerisation [13]. One study has shown
481 Rv2827c upregulation in response to isoniazid and rifampicin treatment, albeit as part of more
482 general TA system upregulation [64].

483

484 The IR conservation between P_{abiEi} and $P_{rv2827c}$ (**Fig. 3**) suggested that autoregulation may also occur
485 in a biochemically comparable manner between the two. However, Rv2827c bound the pairs of
486 inverted repeats with either no co-operativity (**Fig. 4**), or weakly negative co-operativity (**Fig. 5**).
487 There was clear negative co-operativity when all four inverted repeats were tested (**Fig. 6**). Analysing
488 each inverted repeat independently by mutational studies identified significant differences between
489 the Rv2827c-IR dissociation constants (**Fig. 6E-M**). These data have allowed us to propose a model
490 for the regulation of *rv2827c-rv2826c* (**Fig. 8**). As *rv2827c* is needed for normal growth, this suggests
491 that *rv2826c* encodes a toxin capable of causing growth defects [25,65], which is antagonised by
492 Rv2827c (**Fig. 8A**). Expression of *rv2827c-rv2826c* is negatively autoregulated by Rv2827c, and this is
493 made possible by sequential binding of Rv2827c to the four IR sequences, in order as determined by
494 binding affinity (**Fig. 8B**). Given the high concentration of Rv2827c required to saturate the lower
495 affinity site IR3 (**Fig. 6J, K; Fig. 8B**), mimicking the mutational analysis performed here in promoter
496 activity studies would provide useful insight into the function of each IR sequence. These binding
497 events have apparent negative co-operativity, likely due to the variations in IR sequences creating a
498 series of binding steps with ever-decreasing affinity. In order to better understand these negatively
499 co-operative interactions further experiments are required, exploring the role of the Rv2827c CTD
500 and increased inverted repeat spacers, akin to previous work on AbiEi [29].

501

502 Negative cooperativity was an unexpected result given the structural similarities between the N-
503 terminal domains of AbiEi and Rv2827c (**Fig. 2B**), and the similarities of their respective promoter
504 architectures (**Fig. 3**). Examples of negative and positive co-operativity have been found in equal
505 abundance across all organisms [66,67]. Positive co-operativity leads to rapid saturation at a defined,
506 short range of concentrations as seen for *abiE* [29]. In contrast, negative co-operativity of Rv2827c

507 binding would be expected to generate a relatively delayed response, working across a greater range
508 of Rv2827c concentrations [67–69]. This variability in tuning according to concentration could in turn
509 relate to the relative potency of the toxins and dosage required to have an effect in their cognate
510 hosts. This variation is evident when comparing saturation curves of AbiEi and Rv2827c to their
511 cognate full-length promoters (**Fig. 6B and Fig. S2F**). Compared to positive co-operativity, there is
512 relatively little information on the presence of negatively co-operative TA-promoter interactions.
513 However, clear evidence supports weaker binding of un-complexed type II antitoxins [52,70] when
514 compared to the conditionally co-operative binding of TA complexes [28,52,71,72]. It is noteworthy
515 that unlike many type II antitoxins, AbiEi and Rv2827c are fully folded and stable, and also no
516 conditionally co-operative response was seen for AbiE, and so the conditional model proposed for
517 many type II systems likely does not apply [15].

518

519 This study has shown that the similar structures and promoter architectures between AbiEi, Rv2827c
520 (and indeed Rv1044) have been co-opted to form different regulatory modules. A greater
521 understanding of how these nuances of regulation are applied in the cognate hosts may provide
522 greater insight into the control of bacterial growth. Understanding these systems and how they
523 regulate bacterial behaviour is thereby an important step in developing a means to control TA
524 systems towards utilising them for their potential therapeutic value.

525

526

527

528

529

ACKNOWLEDGEMENTS

We thank Koen Semeijn and Ron Dy for initial plasmid construction and preliminary testing.

AUTHOR CONTRIBUTIONS

Conceptualization, all authors; Investigation, I.N.B., B.U., H.H.; Writing, all authors; Funding acquisition, P.C.F., T.R.B.; Supervision, P.C.F., T.R.B..

FUNDING

This work was supported by a Springboard Award from the Academy of Medical Sciences (SBF002\1104) [I.N.B., B.U., T.R.B.], a BBSRC NLD Doctoral Training Partnership studentship [I.N.B.], a University of Otago Doctoral Scholarship [H.G.H], a University of Otago Research Grant [P.C.F], School of Biomedical Sciences Bequest Funds, University of Otago [P.C.F] and the Matariki Network of Universities (MNU) [P.C.F].

CONFLICT OF INTEREST

The authors declare no conflict of interest.

549

550 # REFERENCES

551 [1] J.P. Norton, M.A. Mulvey, Toxin-Antitoxin Systems Are Important for Niche-Specific
552 Colonization and Stress Resistance of Uropathogenic *Escherichia coli*, PLoS Pathog. 8 (2012)
553 e1002954.

554 [2] H. Van Acker, T. Coenye, The Role of Reactive Oxygen Species in Antibiotic-Mediated Killing of
555 Bacteria, Trends Microbiol. 25 (2017) 456–466.

556 [3] S. Helaine, A.M. Cheverton, K.G. Watson, L.M. Faure, S.A. Matthews, D.W. Holden,
557 Internalization of salmonella by macrophages induces formation of nonreplicating persisters,
558 Science. 343 (2014) 204–208.

559 [4] R. Page, W. Peti, Toxin-antitoxin systems in bacterial growth arrest and persistence, Nat.
560 Chem. Biol. (2016).

561 [5] P.C. Fineran, T.R. Blower, I.J. Foulds, D.P. Humphreys, K.S. Lilley, G.P. Salmond, The phage
562 abortive infection system, ToxIN, functions as a protein-RNA toxin-antitoxin pair, Proc. Natl.
563 Acad. Sci. U. S. A. 106 (2009) 894–899.

564 [6] N. Fraikin, F. Goormaghtigh, L. Van Melderen, Type II toxin-antitoxin systems: evolution and
565 revolutions., J. Bacteriol. (2020).

566 [7] S. Szekeres, M. Dauti, C. Wilde, D. Mazel, D.A. Rowe-Magnus, Chromosomal toxin-antitoxin
567 loci can diminish large-scale genome reductions in the absence of selection, Mol. Microbiol.
568 63 (2007) 1588–1605.

569 [8] R.A.F. Wozniak, M.K. Waldor, Integrative and conjugative elements: mosaic mobile genetic
570 elements enabling dynamic lateral gene flow, Nat. Rev. Microbiol. 8 (2010) 552–563.

571 [9] H. Deter, R. Jensen, W. Mather, N. Butzin, Mechanisms for Differential Protein Production in
572 Toxin–Antitoxin Systems, Toxins. 9 (2017) 211.

573 [10] A.M. Hall, B. Gollan, S. Helaine, Toxin–antitoxin systems: reversible toxicity, Curr. Opin.
574 Microbiol. 36 (2017) 102–110.

575 [11] S.J. Labrie, J.E. Samson, S. Moineau, Bacteriophage resistance mechanisms, Nat. Rev.
576 Microbiol. 8 (2010) 317–327.

577 [12] M.C. Chopin, A. Chopin, E. Bidnenko, Phage abortive infection in lactococci: variations on a
578 theme, Curr. Opin. Microbiol. 8 (2005) 473–479.

579 [13] H. Masuda, Q. Tan, N. Awano, K.-P. Wu, M. Inouye, YeeU enhances the bundling of
580 cytoskeletal polymers of MreB and FtsZ, antagonizing the CbtA (YeeV) toxicity in *Escherichia*
581 *coli*, Mol. Microbiol. 84 (2012) 979–989.

582 [14] H. Masuda, Q. Tan, N. Awano, Y. Yamaguchi, M. Inouye, A novel membrane-bound toxin for
583 cell division, CptA (YgfX), inhibits polymerization of cytoskeleton proteins, FtsZ and MreB, in
584 *Escherichia coli*, FEMS Microbiol. Lett. 328 (2012) 174–81.

585 [15] R.L. Dy, R. Przybilski, K. Semeijn, G.P.C. Salmond, P.C. Fineran, A widespread bacteriophage
586 abortive infection system functions through a Type IV toxin-antitoxin mechanism., Nucleic
587 Acids Res. 42 (2014) 4590–605.

588 [16] T.R. Blower, X.Y. Pei, F.L. Short, P.C. Fineran, D.P. Humphreys, B.F. Luisi, G.P.C. Salmond, A
589 processed noncoding RNA regulates an altruistic bacterial antiviral system, Nat. Struct. Mol.
590 Biol. 18 (2011) 185–190.

591 [17] E. Emond, E. Dion, S.A. Walker, E.R. Vedamuthu, J.K. Kondo, S. Moineau, AbiQ, an abortive
592 infection mechanism from *Lactococcus lactis*, Appl. Environ. Microbiol. 64 (1998) 4748–56.

593 [18] J.E. Samson, S. Spinelli, C. Cambillau, S. Moineau, Structure and activity of AbiQ, a lactococcal
594 endoribonuclease belonging to the type III toxin-antitoxin system, Mol. Microbiol. 87 (2013)
595 756–768.

596 [19] D.C. Pecota, T.K. Wood, Exclusion of T4 phage by the hok/sok killer locus from plasmid R1, J.
597 Bacteriol. 178 (1996) 2044–2050.

598 [20] R. Hazan, H. Engelberg-Kulka, *Escherichia coli* mazEF-mediated cell death as a defense
599 mechanism that inhibits the spread of phage P1, Mol. Genet. Genomics. 272 (2004) 227–234.

600 [21] I. Keren, S. Minami, E. Rubin, K. Lewis, Characterization and transcriptome analysis of
601 *Mycobacterium tuberculosis* persisters., MBio. 2 (2011) e00100-11.

602 [22] A. Sala, P. Bordes, P. Genevaux, Multiple toxin-antitoxin systems in *Mycobacterium*
603 *tuberculosis*, Toxins 6 (2014) 1002-1020.

604 [23] R.A. Slayden, C.C. Dawson, J.E. Cummings, Toxin–antitoxin systems and regulatory
605 mechanisms in *Mycobacterium tuberculosis*, Pathog. Dis. 76 (2018).

606 [24] H. Akarsu, P. Bordes, M. Mansour, D.J. Bigot, P. Genevaux, L. Falquet, TASmania: A bacterial
607 Toxin-Antitoxin Systems database, PLoS Comput. Biol. 15 (2019) e1006946.

608 [25] C.M. Sassetti, D.H. Boyd, E.J. Rubin, Genes required for mycobacterial growth defined by high
609 density mutagenesis, Mol. Microbiol. 48 (2003) 77–84.

610 [26] M.A. Dejesus, E.R. Gerrick, W. Xu, S.W. Park, J.E. Long, C.C. Boutte, E.J. Rubin, D.
611 Schnappinger, S. Ehrt, S.M. Fortune, C.M. Sassetti, T.R. Ioerger, Comprehensive essentiality
612 analysis of the *Mycobacterium tuberculosis* genome via saturating transposon mutagenesis,
613 MBio. 8 (2017) e02133-16.

614 [27] K. Gerdes, S.K. Christensen, A. Lobner-Olesen, Prokaryotic toxin-antitoxin stress response loci,

615 Nat. Rev. Microbiol. 3 (2005) 371–382.

616 [28] M. Overgaard, J. Borch, M.G. Jørgensen, K. Gerdes, Messenger RNA interferase RelE controls
617 *relBE* transcription by conditional cooperativity, Mol. Microbiol. 69 (2008) 841–857.

618 [29] H.G. Hampton, S.A. Jackson, R.D. Fagerlund, A.I.M. Vogel, R.L. Dy, T.R. Blower, P.C. Fineran,
619 AbiEi Binds Cooperatively to the Type IV abiE Toxin–Antitoxin Operator Via a Positively-
620 Charged Surface and Causes DNA Bending and Negative Autoregulation, J. Mol. Biol. 430
621 (2018) 1141–1156.

622 [30] R. Janowski, S. Panjikar, A.N. Eddine, S.H.E. Kaufmann, M.S. Weiss, Structural analysis reveals
623 DNA binding properties of Rv2827c, a hypothetical protein from *Mycobacterium tuberculosis*,
624 J. Struct. Funct. Genomics. 10 (2009) 137–150.

625 [31] C. Aslanidis, P.J. de Jong, Ligation-independent cloning of PCR products (LIC-PCR), Nucleic
626 Acids Res. 18 (1990) 6069–74.

627 [32] J. Lodge, J. Fear, S. Busby, P. Gunasekaran, N.R. Kamini, Broad host range plasmids carrying
628 the *Escherichia coli* lactose and galactose operons, FEMS Microbiol Lett. 95 (1992) 271–276.

629 [33] W. Kabsch, XDS., Acta Crystallogr. D. Biol. Crystallogr. 66 (2010) 125–32.

630 [34] W. Kabsch, Integration, scaling, space-group assignment and post-refinement, Acta
631 Crystallogr. D. Biol. Crystallogr. 66 (2010) 133–44.

632 [35] M.D. Winn, C.C. Ballard, K.D. Cowtan, E.J. Dodson, P. Emsley, P.R. Evans, R.M. Keegan, E.B.
633 Krissinel, A.G.W. Leslie, A. McCoy, S.J. McNicholas, G.N. Murshudov, N.S. Pannu, E.A.
634 Potterton, H.R. Powell, R.J. Read, A. Vagin, K.S. Wilson, Overview of the CCP4 suite and
635 current developments, Acta Crystallogr. D. Biol. Crystallogr. 67 (2011) 235–42.

636 [36] G.M. Sheldrick, IUCr, A short history of *SHELX*, Acta Crystallogr. Sect. A Found. Crystallogr. 64

637 (2008) 112–122.

638 [37] A.A. Vagin, R.A. Steiner, A.A. Lebedev, L. Potterton, S. McNicholas, F. Long, G.N. Murshudov,
639 *REFMAC* 5 dictionary: organization of prior chemical knowledge and guidelines for its use,
640 Acta Crystallogr. Sect. D Biol. Crystallogr. 60 (2004) 2184–2195.

641 [38] K. Cowtan, IUCr, The Buccaneer software for automated model building. 1. Tracing protein
642 chains, Acta Crystallogr. Sect. D Biol. Crystallogr. 62 (2006) 1002–1011.

643 [39] P.D. Adams, P. V Afonine, G. Bunkóczi, V.B. Chen, I.W. Davis, N. Echols, J.J. Headd, L.-W. Hung,
644 G.J. Kapral, R.W. Grosse-Kunstleve, A.J. McCoy, N.W. Moriarty, R. Oeffner, R.J. Read, D.C.
645 Richardson, J.S. Richardson, T.C. Terwilliger, P.H. Zwart, PHENIX: a comprehensive Python-
646 based system for macromolecular structure solution, Acta Crystallogr. D. Biol. Crystallogr. 66
647 (2010) 213–21.

648 [40] P. Emsley, K. Cowtan, Coot: model-building tools for molecular graphics, Acta Crystallogr D
649 Biol Crystallogr. 60 (2004) 2126–2132.

650 [41] S. Gore, S. Velankar, G.J. Kleywegt, Implementing an X-ray validation pipeline for the Protein
651 Data Bank, Acta Crystallogr. Sect. D Biol. Crystallogr. 68 (2012) 478–483.

652 [42] J. Pei, B.-H. Kim, N. V. Grishin, PROMALS3D: a tool for multiple protein sequence and
653 structure alignments, Nucleic Acids Res. 36 (2008) 2295–2300.

654 [43] F. Madeira, Y. mi Park, J. Lee, N. Buso, T. Gur, N. Madhusoodanan, P. Basutkar, A.R.N. Tivey,
655 S.C. Potter, R.D. Finn, R. Lopez, The EMBL-EBI search and sequence analysis tools APIs in
656 2019, Nucleic Acids Res. 47 (2019) W636–W641.

657 [44] G.E. Crooks, G. Hon, J.-M. Chandonia, S.E. Brenner, WebLogo: A Sequence Logo Generator,
658 Genome Res. 14 (2004) 1188-1190.

659 [45] J. Schaefer, G. Jovanovic, I. Kotta-Loizou, M. Buck, A data comparison between a traditional
660 and the single-step β-galactosidase assay, Data Br. 8 (2016) 350–352.

661 [46] J. Schaefer, G. Jovanovic, I. Kotta-Loizou, M. Buck, Single-step method for β-galactosidase
662 assays in *Escherichia coli* using a 96-well microplate reader, Anal. Biochem. 503 (2016) 56–57.

663 [47] K.S. Gajiwala, S.K. Burley, Winged helix proteins, Curr. Opin. Struct. Biol. 10 (2000) 110–116.

664 [48] L. Holm, C. Sander, Protein structure comparison by alignment of distance matrices, J. Mol.
665 Biol. 233 (1993) 123–138.

666 [49] H. Chen, H.-X. Zhou, Prediction of interface residues in protein-protein complexes by a
667 consensus neural network method: Test against NMR data, Proteins Struct. Funct.
668 Bioinforma. 61 (2005) 21–35.

669 [50] R.K. Umarov, V. V. Solovyev, Recognition of prokaryotic and eukaryotic promoters using
670 convolutional deep learning neural networks, PLoS One. 12 (2017) e0171410.

671 [51] S. Rodrigue, J. Brodeur, P.-E. Jacques, A.L. Gervais, R. Brzezinski, L. Gaudreau, Identification of
672 mycobacterial sigma factor binding sites by chromatin immunoprecipitation assays, J.
673 Bacteriol. 189 (2007) 1505–13.

674 [52] M. V. Merfa, B. Niza, M.A. Takita, A.A. De Souza, The MqsRA Toxin-Antitoxin System from
675 *Xylella fastidiosa* Plays a Key Role in Bacterial Fitness, Pathogenicity, and Persister Cell
676 Formation, Front. Microbiol. 7 (2016) 904.

677 [53] V.W.C. Soo, T.K. Wood, Antitoxin MqsA Represses Curli Formation Through the Master
678 Biofilm Regulator CsgD, Sci. Rep. 3 (2013) 3186.

679 [54] X. Wang, T.K. Wood, Toxin-antitoxin systems influence biofilm and persister cell formation
680 and the general stress response, Appl. Env. Microbiol. 77 (2011) 5577–5583.

681 [55] N. Agarwal, A.K. Tyagi, Mycobacterial transcriptional signals: requirements for recognition by
682 RNA polymerase and optimal transcriptional activity, Nucleic Acids Res. 34 (2006) 4245–57.

683 [56] S.S. Shell, J. Wang, P. Lapierre, M. Mir, M.R. Chase, M.M. Pyle, R. Gawande, R. Ahmad, D.A.
684 Sarracino, T.R. Ioerger, S.M. Fortune, K.M. Derbyshire, J.T. Wade, T.A. Gray, Leaderless
685 Transcripts and Small Proteins Are Common Features of the Mycobacterial Translational
686 Landscape, PLoS Genet. 11 (2015) e1005641.

687 [57] T. Cortes, O.T. Schubert, G. Rose, K.B. Arnvig, I. Comas, R. Aebersold, D.B. Young, Genome-
688 wide mapping of transcriptional start sites defines an extensive leaderless transcriptome in
689 *Mycobacterium tuberculosis*, Cell Rep. 5 (2013) 1121–31.

690 [58] P. Sachdeva, R. Misra, A.K. Tyagi, Y. Singh, The sigma factors of *Mycobacterium tuberculosis*:
691 regulation of the regulators, FEBS J. 277 (2010) 605–626.

692 [59] T.R. Rustad, K.J. Minch, S. Ma, J.K. Winkler, S. Hobbs, M. Hickey, W. Brabant, S. Turkarslan,
693 N.D. Price, N.S. Baliga, D.R. Sherman, Mapping and manipulating the *Mycobacterium*
694 *tuberculosis* transcriptome using a transcription factor overexpression-derived regulatory
695 network, Genome Biol. 15 (2014) 502.

696 [60] S. Wu, S.T. Howard, D.L. Lakey, A. Kipnis, B. Samten, H. Safi, V. Gruppo, B. Wizel, H. Shams,
697 R.J. Basaraba, I.M. Orme, P.F. Barnes, The principal sigma factor sigA mediates enhanced
698 growth of *Mycobacterium tuberculosis in vivo*, Mol. Microbiol. 51 (2004) 1551–1562.

699 [61] A.J. Vallecillo, C. Espitia, Expression of Mycobacterium tuberculosis pe_pgrs33 is repressed
700 during stationary phase and stress conditions, and its transcription is mediated by sigma
701 factor A, Microb. Pathog. 46 (2009) 119–127.

702 [62] G. Bagchi, S. Chauhan, D. Sharma, J.S. Tyagi, Transcription and autoregulation of the Rv3134c-
703 devR-devS operon of *Mycobacterium tuberculosis*, Microbiology. 151 (2005) 4045–4053.

704 [63] J. Rengarajan, B.R. Bloom, E.J. Rubin, Genome-wide requirements for Mycobacterium
705 tuberculosis adaptation and survival in macrophages, Proc. Natl. Acad. Sci. U. S. A. 102 (2005)
706 8327–8332.

707 [64] A. Gupta, B. Venkataraman, M. Vasudevan, K. Gopinath Bankar, Co-expression network
708 analysis of toxin-antitoxin loci in *Mycobacterium tuberculosis* reveals key modulators of
709 cellular stress, Sci. Rep. 7 (2017) 5868.

710 [65] J.E. Griffin, J.D. Gawronski, M.A. Dejesus, T.R. Ioerger, B.J. Akerley, C.M. Sassetti, High-
711 resolution phenotypic profiling defines genes essential for mycobacterial growth and
712 cholesterol catabolism, PLoS Pathog. 7 (2011) e1002251.

713 [66] D.E. Koshland, K. Hamadani, Proteomics and Models for Enzyme Cooperativity, J. Biol. Chem.
714 277 (2002) 46841–46844.

715 [67] A. Levitzki, D.E. Koshland, Negative cooperativity in regulatory enzymes, Proc. Natl. Acad. Sci.
716 U. S. A. 62 (1969) 1121–1128.

717 [68] P. De Meyts, J. Roth, Cooperativity in ligand binding: A new graphic analysis, Biochem.
718 Biophys. Res. Commun. 66 (1975) 1118–1126.

719 [69] S.H. Ha, J.E. Ferrell, Jr., Thresholds and ultrasensitivity from negative cooperativity, Science.
720 352 (2016) 990–993.

721 [70] M. Overgaard, J. Borch, K. Gerdes, RelB and RelE of Escherichia coli Form a Tight Complex
722 That Represses Transcription via the Ribbon–Helix–Helix Motif in RelB, J. Mol. Biol. 394 (2009)
723 183–196.

724 [71] I. Cataudella, A. Trusina, K. Sneppen, K. Gerdes, N. Mitarai, Conditional cooperativity in toxin–
725 antitoxin regulation prevents random toxin activation and promotes fast translational

726 recovery, Nucleic Acids Res. 40 (2012) 6424–6434.

727 [72] A. Garcia-Pino, S. Balasubramanian, L. Wyns, E. Gazit, H. De Greve, R.D. Magnuson, D.
728 Charlier, N.A. van Nuland, R. Loris, Allostery and intrinsic disorder mediate transcription
729 regulation by conditional cooperativity, Cell. 142 (2010) 101–111.

730

731

732

733

734

735

736

737

738

739

740

741

742

743

744

745 # FIGURES

746 **Fig. 1.** Antitoxin AbiEi is a two-domain protein with bilateral opposingly-charged faces. (A) Scaled
747 representation of the four *M. tuberculosis* TA systems containing NTase-like toxin
748 genes and AbiE from *S. agalactiae*. Numbers in parentheses indicate amino acid length. All
749 five toxins are DUF1814 proteins; Rv1044, Rv2827c and AbiEi are COG5340-containing antitoxins.
750 Putative antitoxin Rv0837c is a COG4861 protein and the significantly shorter putative antitoxin
751 Rv0078B is unclassified. The four *M. tuberculosis* systems were re-named as shown.
752 (B) AbiEi antitoxin structure shown in pink cartoon representation, in two views rotated 180°. (C)
753 Electrostatic potential of AbiEi, posed as per (B), with electropositive charge in blue and
754 electronegative charge in red. (D) Previously solved Rv2827c structure shown in blue cartoon
755 representation, in two views rotated 180° (PDB: 1ZEL). (E) Electrostatic potential of Rv2827c, posed
756 as per (D), colored as per (C).
757
758

759 **Fig. 2**. AbiEi and Rv2827c are structurally similar, but have been captured in different positions with
760 differing predicted protein interaction interfaces. (A) AbiEi (pink) and Rv2827c (blue) in cartoon
761 representation, aligned via the N-terminal winged helix-turn-helix domains, shown as two
762 orthogonal views. The positions of the C-terminal domains diverge at a 65° angle. (B) Close-up
763 structural superposition of the isolated N-terminal helices of AbiEi and Rv2827c, colored as per (A).
764 The three helices (H1-3) of the N-terminal winged helix-turn-helix domains align well. (C) Close-up
765 structural superposition of the isolated C-terminal domains of AbiEi and Rv2827c, colored as per (A).
766 The core secondary structural features of the C-terminal domains approximate to the same
767 positions, but the Rv2827c C-terminal domain has additional features at the C-terminus. (D)
768 AbiEi has C-terminal residues predicted to be involved in making protein-protein interactions, which
769 might allow positive co-operativity in AbiEi monomer binding. AbiEi is in pink cartoon
770 representation with identified interacting residues in red, and is shown in orthogonal views. (E)
771 Rv2827c does not have an equivalent patch of C-terminal interacting residues. Rv2827c is in blue
772 cartoon representation, with identified interacting residues in cyan, and is shown in 180° rotation.
773 Residues were identified using the cons-PPISP server. Rv2827c PDB code: 1ZEL.
774

775

776 **Fig. 3.** The *rv2827c-rv2826c* promoter has similar features but is more complex than
777 the *abiE* promoter. (A) Cartoon of the *abiE* and *rv2827c-rv2826c* promoters (pink and blue,
778 respectively), showing the relative positions of the 23 bp inverted repeats (IRs). Putative
779 transcriptional -35, -10 and start sites, along with ribosome binding sites (RBS), are indicated where
780 possible. (B) Alignment of the six, 23 bp, IR sequences shows consensus sequences between
781 the *abiE* and *rv2827c-rv2826c* promoters. The alignment was made using MView and the consensus
782 was made using WebLogo.

783

784 **Fig. 4.** Rv2827c binds non-co-operatively to the IR3-IR4 region of the *rv2827c-rv2826c* promoter. (A)
785 Sequence level cartoon of the fluorescently labelled probe containing IR3-IR4, with -35, -10 and
786 transcriptional start indicated. (B) Electrophoretic mobility shift assay (EMSA) of titrated
787 Rv2827c with the probe in (A). (C) EMSA of titrated Rv2827c with the probe in (A) altered by
788 replacing IR4 with polyC. (D) EMSA of titrated Rv2827c with the probe in (A) altered by replacing IR3
789 with polyC. (E) EMSA of titrated Rv2827c with the probe in (A) altered by replacing both IR3 and IR4

790 with polyC. For (B-E); protein concentrations are shown on each panel together with the binding
791 events (0, 1 or 2); S – each experiment contained 100-fold excess of the specific unlabelled probe; NS
792 – each experiment contained 100-fold excess of non-specific unlabelled probe; numbering -1 to -71
793 denotes the promoter region included in the probe, upstream of the translational start site in order
794 to include all of IR4. (F) Fractional saturation curve plotted using the EMSA data of (B). (G) Hill plot
795 using the EMSA data from (B). For (F) and (G), points are plotted from triplicate data and display
796 mean values with standard error of the mean.

797

798 **Fig. 5**. Rv2827c binds with weak negative co-operativity to the IR1-IR2 region of the *rv2827c-*
799 *rv2826c* promoter. (A) Sequence level cartoon of the fluorescently labelled probe containing IR1-IR2.
800 (B) Electrophoretic mobility shift assay (EMSA) of titrated Rv2827c with the probe in (A). (C) EMSA of
801 titrated Rv2827c with the probe in (A) altered by replacing IR2 with polyC. (D) EMSA of titrated
802 Rv2827c with the probe in (A) altered by replacing IR1 with polyC. (E) EMSA of titrated Rv2827c with
803 the probe in (A) altered by replacing both IR1 and IR2 with polyC. For (B-E); protein concentrations
804 are shown on each panel together with the binding events (0, 1 or 2); S – each experiment contained
805 100-fold excess of the specific unlabelled probe; NS – each experiment contained 100-fold excess of
806 non-specific unlabelled probe; numbering -60 to -131 denotes the promoter region included in the
807 probe. (F) Fractional saturation curve plotted using the EMSA data of (B). (G) Hill plot using the EMSA
808 data from (B). For (F) and (G), points are plotted from triplicate data and display mean values
809 with standard error of the mean.

810

811 **Fig. 6**. Rv2827c binds with negative co-operativity to the full *rv2827c-rv2826c* promoter. (A) EMSA of
812 titrated Rv2827c with a probe covering from -1 to -131 of the r*v2827c-rv2826c* promoter, covering
813 IR1 to IR4. The titration was performed across two EMSA gels, with an additional zero protein lane
814 included in the second gel for normalization. Protein concentrations are shown below each gel
815 together with the binding events (0, 1, 2, 3 or 4); S – each experiment contained 100-fold excess of
816 the specific unlabelled probe; NS – each experiment contained 100-fold excess of non-specific
817 unlabelled probe. (B) Fractional saturation curve plotted using the EMSA data of (A). (C) Hill plot
818 using the EMSA data from (A). (D) Semi-log saturation curve plotted using the EMSA data of (A),
819 showing distinct breaks in the binding curve, in accordance with the multiple binding sites contained
820 in the probe. (E) Sequence level cartoon of the fluorescently labelled probe containing r*v2827c-*
821 *rv2826c* -1 to -131. (F-M) Saturation curves (F, H, J, L) and Hill plots (G, I, K, M) for each IR calculated
822 using individual IR data gathered using mutant probes (**Fig. 4C and D, Fig. 5C and D**). For (B-D) and
823 (F-M), points are plotted from triplicate data and display mean values with standard error of the
824 mean.
825
826

827 **Fig. 7.** Rv2827c-Rv2826c is a negatively autoregulating system in *E. coli*. (A) Promoter activity from
828 upstream promoter regions of *abiE* (99 bp), and *rv2827c-rv2826c* and *rv1044-rv1045* (500 bp for
829 both) detected using *lacZ* transcriptional fusions. Both the *abiE* and *rv2827c-rv2826c* constructs are
830 active, but the *rv1044-rv1045* construct is not. Plotted data are normalized to the vector-only
831 control. (B) Autoregulation of promoter activity by antitoxins. LacZ activity was measured from
832 the *abiE* and *rv2827c-rv2826c* constructs with or without induction of the cognate antitoxin (AT,
833 ±IPTG). Both AbiE and Rv2827c negatively autoregulate expression. Plotted data are normalized to
834 the uninduced vector-only control. All data (A-C) are plotted as the means of triplicate data, and
835 error bars show standard deviations from the mean.

836

837 **Fig. 8**. Proposed model for negative autoregulation caused by Rv2827c binding to the four *rv2827c-*
838 *rv2826c* promoter inverted repeats. (A) Schematic representation of the putative rv2827c-rv2826c
839 type IV toxin-antitoxin system. Model shows both *rv2827c* and *rv2826c* being translated into the
840 antagonistic antitoxin and toxin protein pair respectively. The antitoxin, Rv2827c has a second
841 function and binds to the *rv2827c-rv2826c* promoter, negatively autoregulating the operon. (B) An
842 order of binding is created by the distinct affinity values for the inverted repeats represented in the
843 sequence level cartoon, calculated from individual IR data gathered using mutant probes (**Fig. 4C** and
844 **D**, **Fig. 5C** and **D**). Rv2827c binds negatively co-operatively, initially to IR1 (0.0205 µM) followed by
845 IR4 (0.121 µM), IR2 (0.862 µM) and finally IR3 (11.0 µM).
846

847

848

849

850

851

852

853

854

855

856

857

858

859

860

861

862

863

864

865

866

867

868

TABLES

Table 1. Crystallographic Data Collection and Refinement Statistics

	AbiEi Native	AbiEi Se-Peak	AbiEi Se-High Remote
PDB ID Code	6Y8Q	-	-
Number of crystals	3	2	1
Beamline	Diamond I03	Diamond I03	Diamond I03
Wavelength, Å	0.9763	0.9793	0.9641
Resolution range, Å	42.11 – 1.83 (1.86 – 1.83)[a]	42.58 – 2.14 (2.19 – 2.14)	53.57 – 2.17 (2.23 – 2.17)
Space group	P1	P1	P1
Unit cell, *a b c* (Å), α β γ (°)	34.24 80.85 122.17, 102.48 96.74 100.47	34.78 81.37 122.99, 101.72 97.18 101.16	34.85 81.38 123.00, 101.74 97.31 101.19
Total reflections	207238 (10275)	443813 (13873)	129874 (8557)
Unique reflections	106620 (5213)	69714 (4469)	65917 (4312)
Multiplicity	1.9	6.4	2.0
Completeness (%)	97.4 (96.1)	99.0 (97.1)	97.9 (91.9)
Mean I/sigma(I)	7.6	6.9	6.1
R_{merge}	0.038 (0.691)	0.169 (1.036)	0.080 (0.593)
R_{meas}	0.053 (0.977)	0.184 (1.260)	0.113 (0.839)
$CC_{1/2}$	0.999 (0.471)	0.991 (0.463)	0.992 (0.599)
R_{work}	0.1812 (0.2812)	-	-
R_{free}	0.2092 (0.3100)	-	-
No. of non-hydrogen atoms	7116	-	-
Macromolecules	6397	-	-
Ligands	62	-	-
Solvent	657	-	-
Protein Residues	769	-	-
RMSD (bonds, Å)	0.012	-	-
RMSD (angles, °)	1.32	-	-
Ramachandran favored (%)	98.68	-	-
Ramachandran allowed (%)	1.32	-	-
Ramachandran outliers (%)	0.00	-	-
Average B-factor	39.61	-	-
Macromolecules	39.04	-	-
Ligands	46.01	-	-
Solvent	44.60	-	-

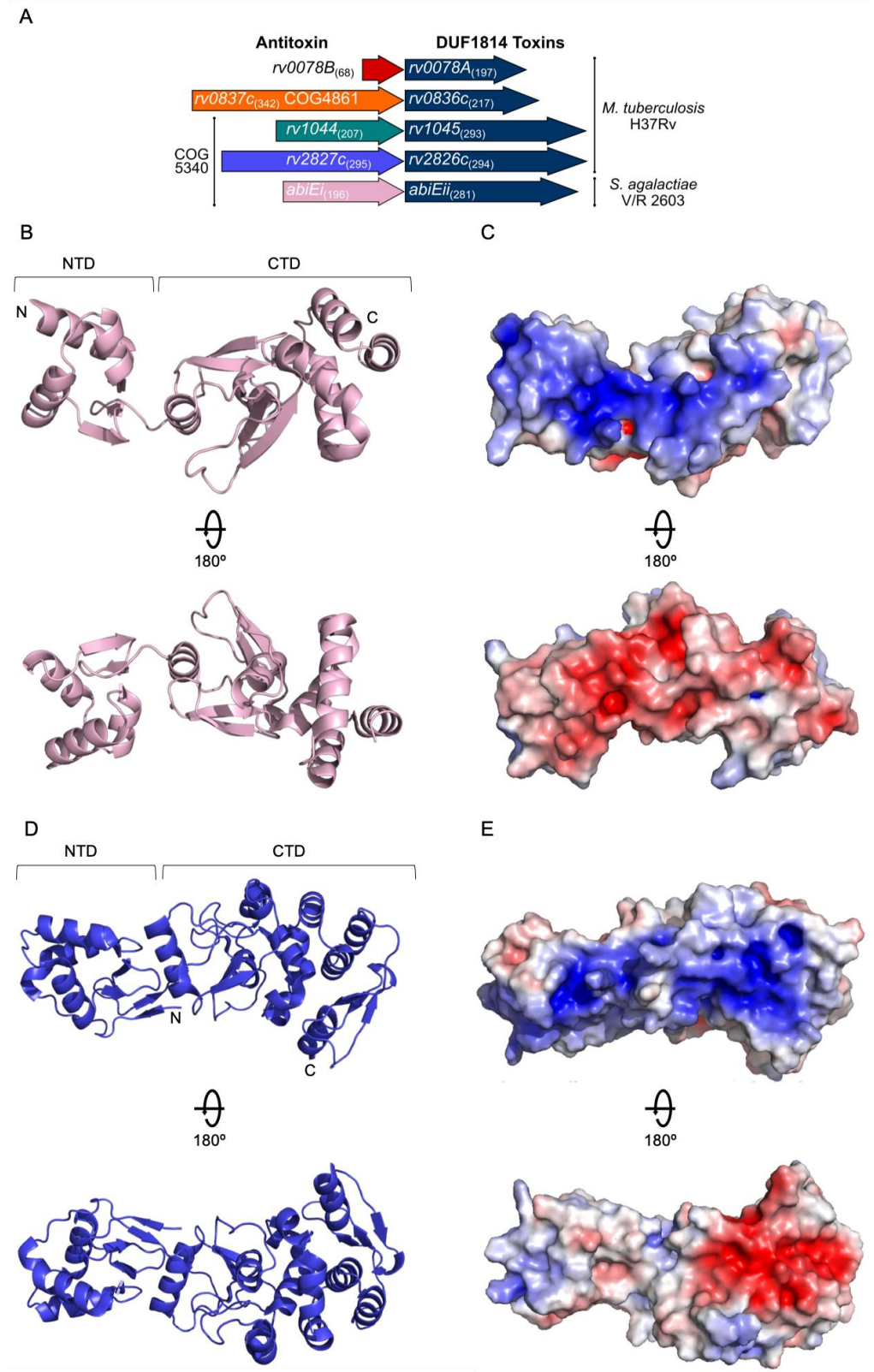
A
Antitoxin
DUF1814 Toxins
rv0078B(68)
rv0078A(197)
rv0837c(342) COG4861
rv0836c(217)
rv1044(207)
rv1045(293)
rv2827c(295)
rv2826c(294)
abiEi(196)
abiEii(281)
COG 5340
M. tuberculosis H37Rv
S. agalactiae V/R 2603
B
NTD
CTD
N
C
180º
C
180º
D
NTD
CTD
N
C
180º
E
180º

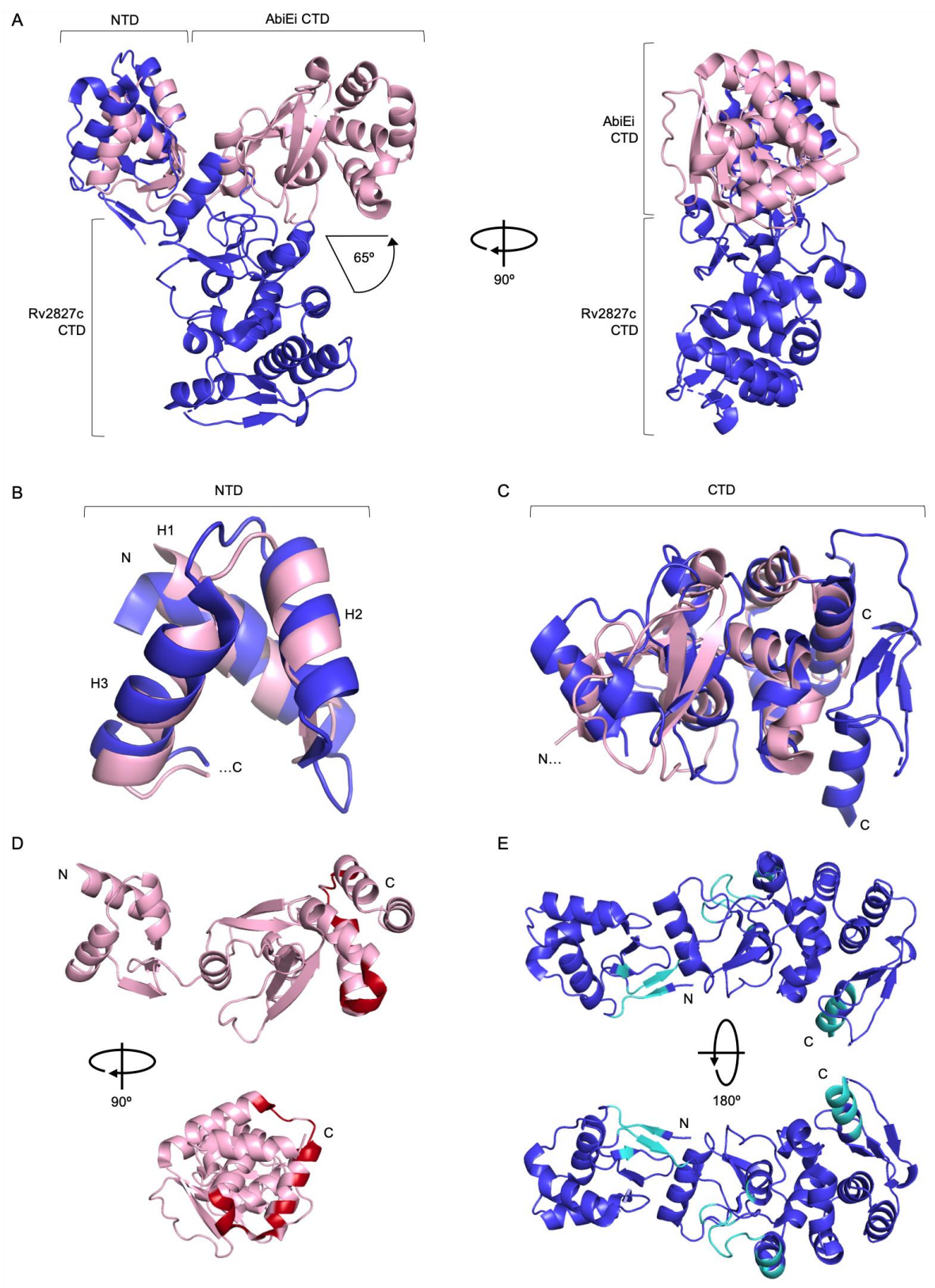
A
NTD
AbiEi CTD
65º
Rv2827c
CTD
90º
AbiEi
CTD
Rv2827c
CTD
B
NTD
H1
N
H2
H3
...C
C
CTD
C
N...
C
D
N
C
90º
C
E
N
C
180º
C
N

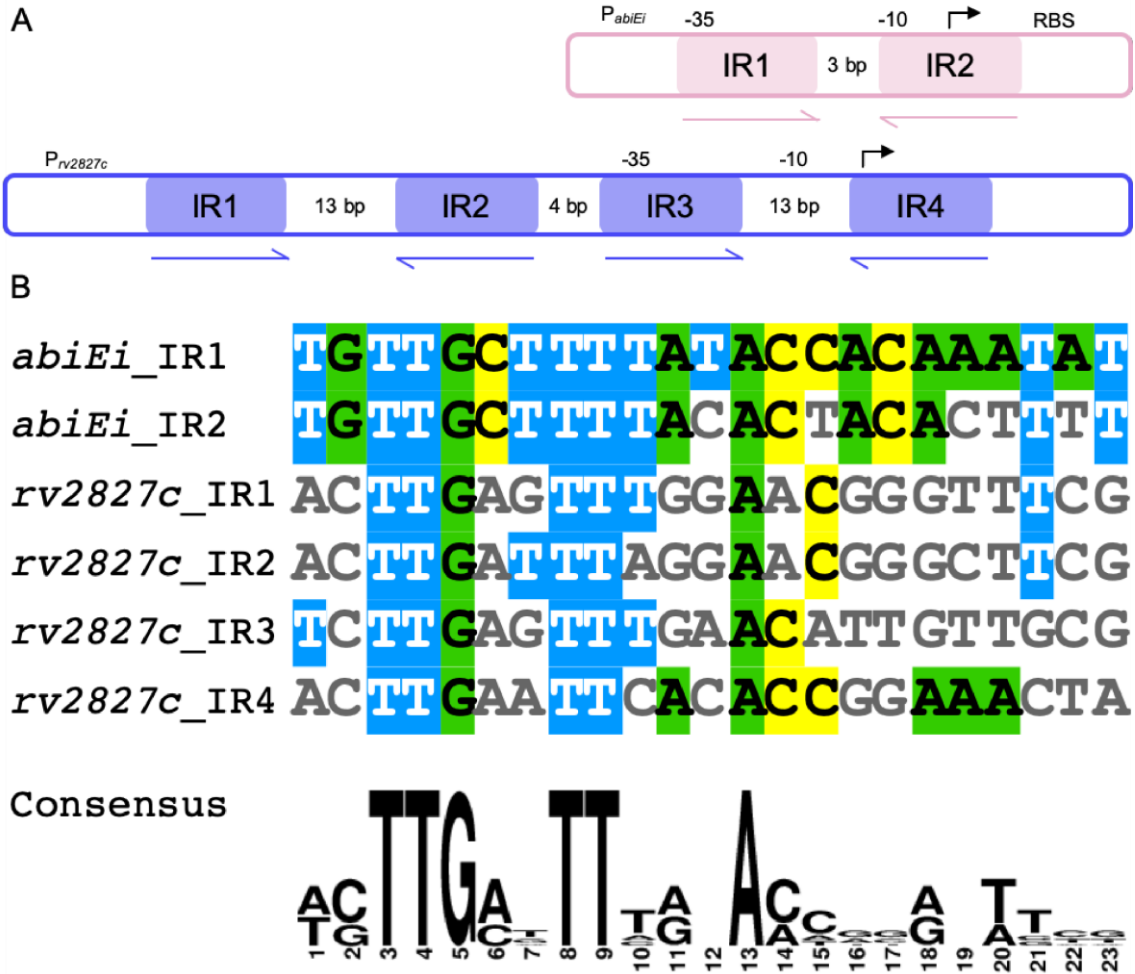
A
PabiEi
-35
-10
RBS
IR1
3 bp
IR2
Prv2827c
-35
-10
IR1
13 bp
IR2
4 bp
IR3
13 bp
IR4
B
abiEi_IR1 TGTTGCTTTTATACCACAAATAT
abiEi_IR2 TGTTGCTTTTACACTACACTTTT
rv2827c_IR1 ACTTGAGTTTGGAACGGGTTCG
rv2827c_IR2 ACTTGATTTAGGAACGGGCTCG
rv2827c_IR3 TCTTGAGTTTGAACATTGTTGCG
rv2827c_IR4 ACTTGAATTCACACCGGAAACTA
Consensus
1 2 3 4 5 6 7 8 9 10 11 12 13 14 15 16 17 18 19 20 21 22 23

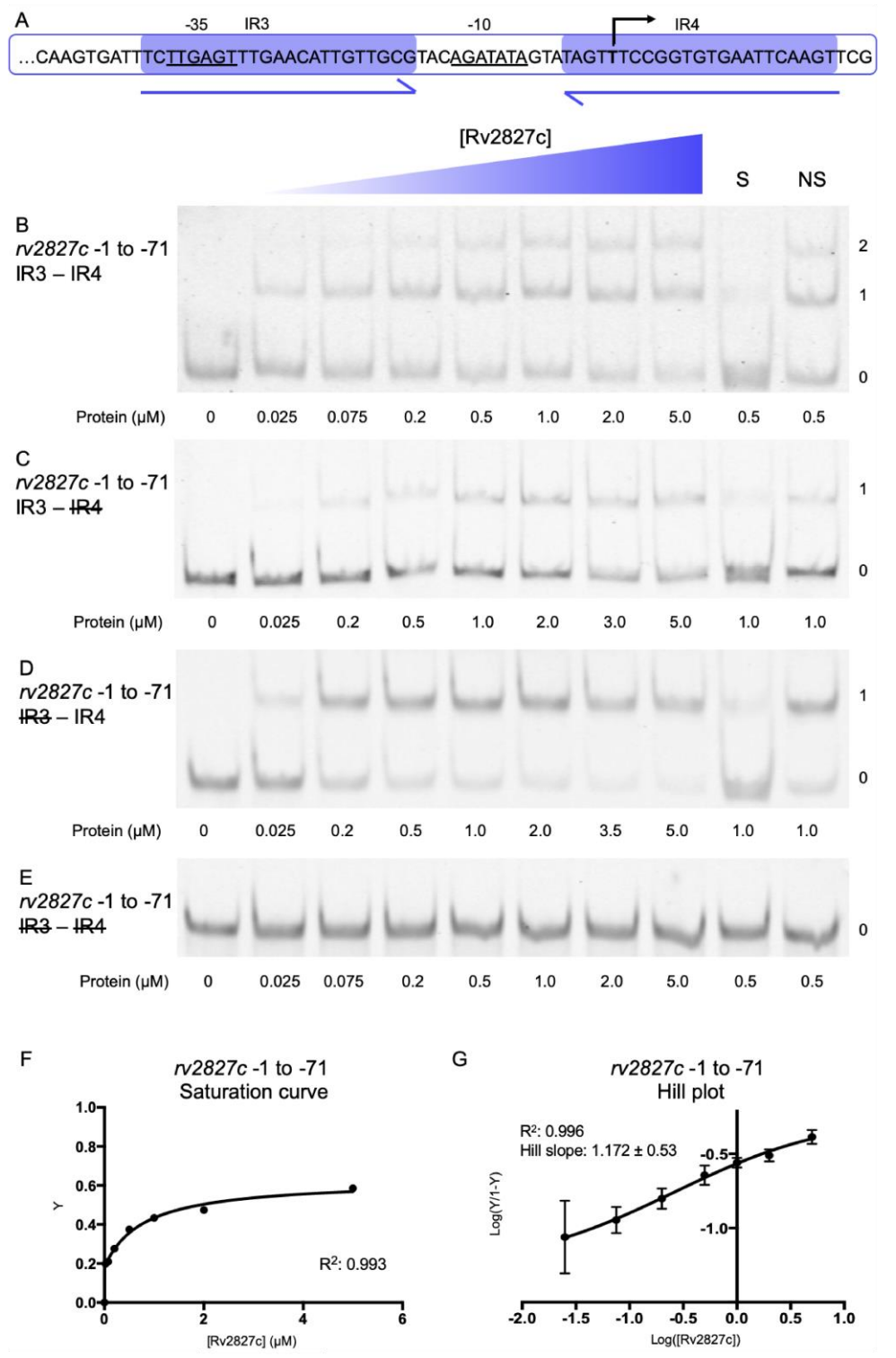
A
-35
IR3
-10
IR4
...CAAGTGATTTCTTGAGTTTGAACATTGTTGCGTACAGATATAGTATAGTTTCCGGTGTGAATTCAAGTTCG
[Rv2827c]
S
NS
B
rv2827c -1 to -71
IR3 – IR4
Protein (μM) 0 0.025 0.075 0.2 0.5 1.0 2.0 5.0 0.5 0.5
C
rv2827c -1 to -71
IR3 – IR4
Protein (μM) 0 0.025 0.2 0.5 1.0 2.0 3.0 5.0 1.0 1.0
D
rv2827c -1 to -71
IR3 – IR4
Protein (μM) 0 0.025 0.2 0.5 1.0 2.0 3.5 5.0 1.0 1.0
E
rv2827c -1 to -71
IR3 – IR4
Protein (μM) 0 0.025 0.075 0.2 0.5 1.0 2.0 5.0 0.5 0.5
F
rv2827c -1 to -71
Saturation curve
Y
R2: 0.993
[Rv2827c] (μM)
G
rv2827c -1 to -71
Hill plot
R2: 0.996
Hill slope: 1.172 ± 0.53
Log(Y/1-Y)
Log([Rv2827c])

A

IR1 IR2

…CAGGGCACTTGAGTTTGGAACGGGTTTCGTACTGTCACTGACCGAAGCCCGTTCCTAAATCAAGTGATTTC

[Rv2827c]

S NS

B

rv2827c -60 to -131 IR1 – IR2

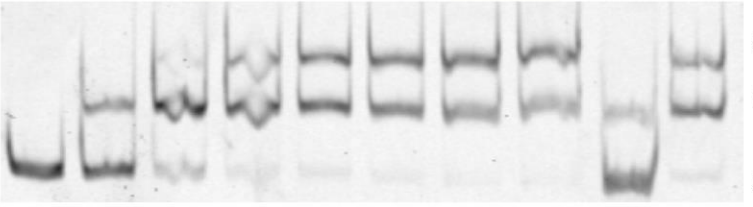

Protein (μM)	0	0.025	0.075	0.2	0.5	1.0	2.0	5.0	0.5	0.5

C

rv2827c -60 to -131 IR1 – ~~IR2~~

Protein (μM)	0	0.0078	0.015	0.03	0.0625	0.125	0.25	0.5	0.25	0.25

D

rv2827c -60 to -131 ~~IR1~~ – IR2

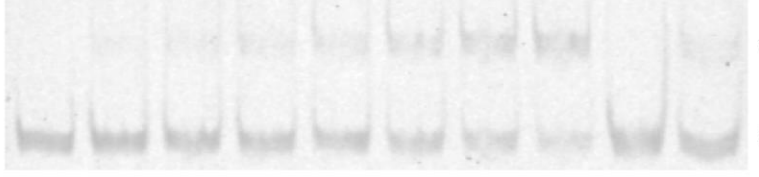

Protein (μM)	0	0.0125	0.025	0.05	0.075	0.2	0.5	2.0	0.075	0.075

E

rv2827c -60 to -131 ~~IR1~~ – ~~IR2~~

Protein (μM)	0	0.025	0.075	0.2	0.5	1.0	2.0	5.0	0.5	0.5

F

rv2827c -60 to -131
Saturation curve

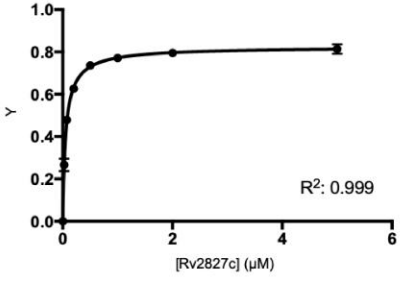

G

rv2827c -60 to -131
Hill plot

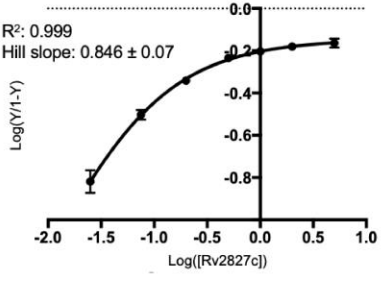

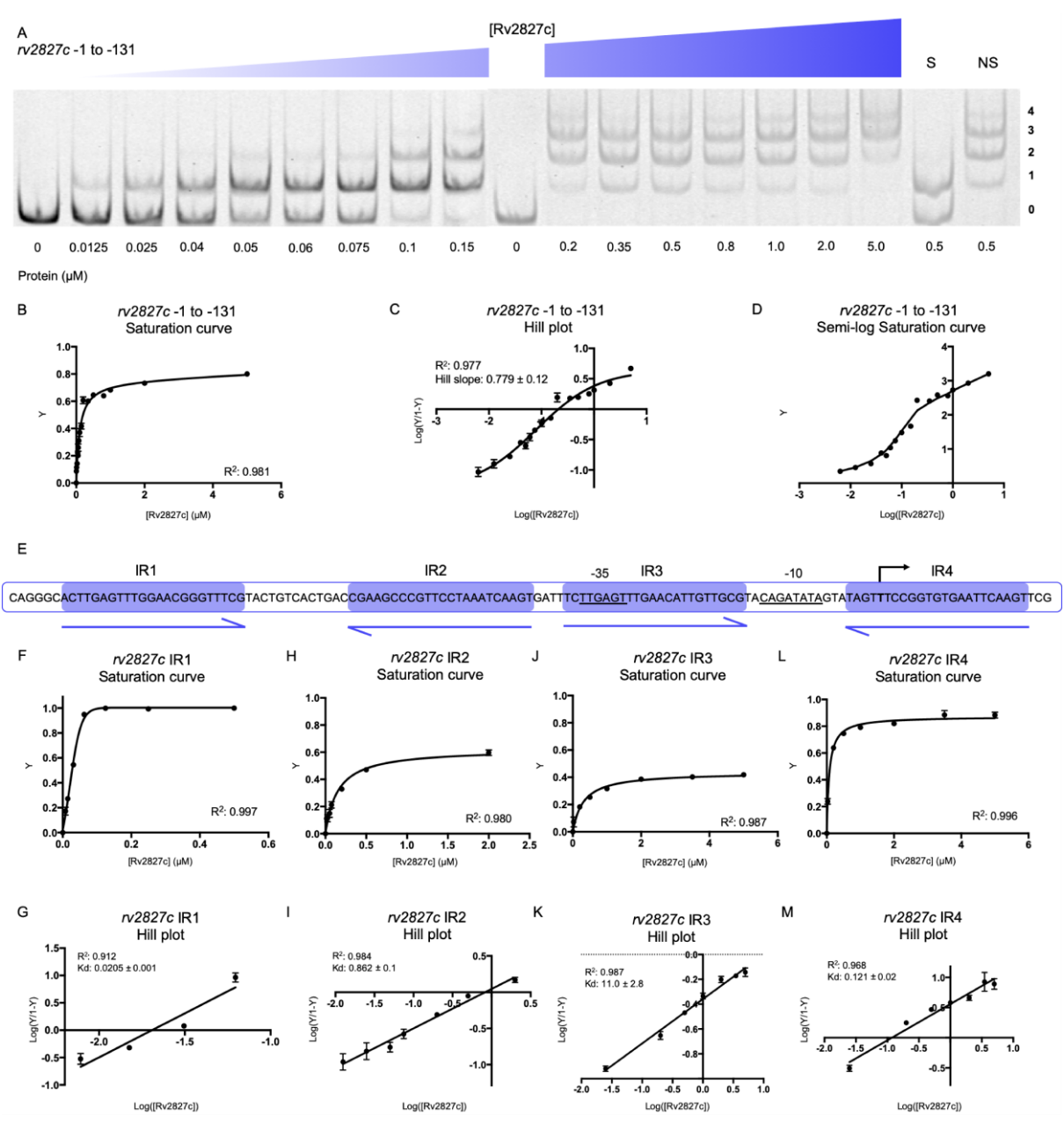
A
rv2827c -1 to -131
[Rv2827c]
S
NS
4
3
2
1
0
0 0.0125 0.025 0.04 0.05 0.06 0.075 0.1 0.15 0 0.2 0.35 0.5 0.8 1.0 2.0 5.0 0.5 0.5
Protein (μM)
B
rv2827c -1 to -131
Saturation curve
Y
R2: 0.981
[Rv2827c] (μM)
C
rv2827c -1 to -131
Hill plot
R2: 0.977
Hill slope: 0.779 ± 0.12
Log(Y/1-Y)
Log([Rv2827c])
D
rv2827c -1 to -131
Semi-log Saturation curve
Y
Log([Rv2827c])
E
IR1
IR2
-35
IR3
-10
IR4
CAGGGCACTTGAGTTTGGAACGGGTTTCGTACTGTCACTGACCGAAGCCCGTTCCTAAATCAAGTGATTTCTTGAGTTTGAACATTGTTGCGTACAGATATAGTATAGTTTCCGGTGTGAATTCAAGTTCG
F
rv2827c IR1
Saturation curve
Y
R2: 0.997
[Rv2827c] (μM)
H
rv2827c IR2
Saturation curve
Y
R2: 0.980
[Rv2827c] (μM)
J
rv2827c IR3
Saturation curve
Y
R2: 0.987
[Rv2827c] (μM)
L
rv2827c IR4
Saturation curve
Y
R2: 0.996
[Rv2827c] (μM)
G
rv2827c IR1
Hill plot
R2: 0.912
Kd: 0.0205 ± 0.001
Log(Y/1-Y)
Log([Rv2827c])
I
rv2827c IR2
Hill plot
R2: 0.984
Kd: 0.862 ± 0.1
Log(Y/1-Y)
Log([Rv2827c])
K
rv2827c IR3
Hill plot
R2: 0.987
Kd: 11.0 ± 2.8
Log(Y/1-Y)
Log([Rv2827c])
M
rv2827c IR4
Hill plot
R2: 0.968
Kd: 0.121 ± 0.02
Log(Y/1-Y)
Log([Rv2827c])

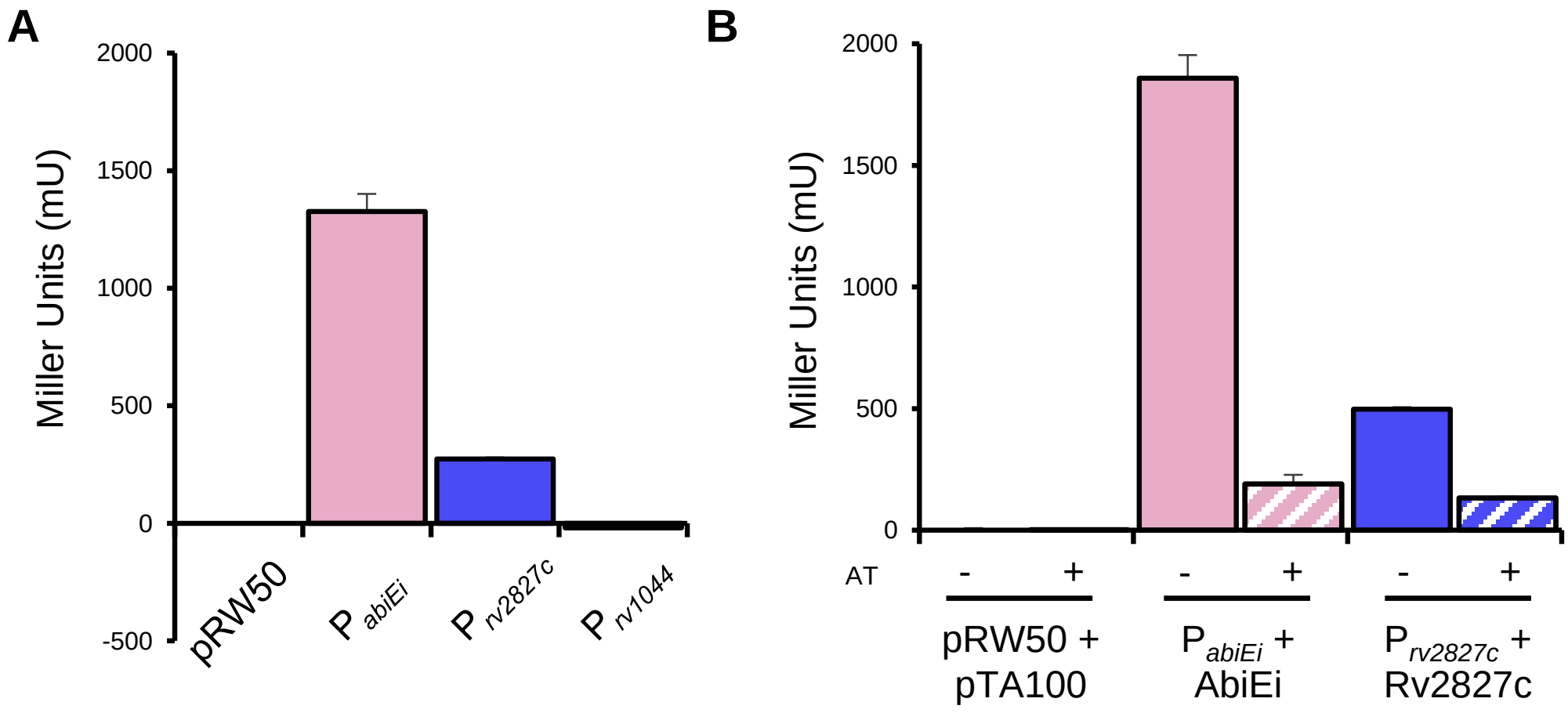
A
Miller Units (mU)
2000
1500
1000
500
0
-500
pRW50
P abiEi
P rv2827c
P rv1044
B
Miller Units (mU)
2000
1500
1000
500
0
AT
-
+
-
+
-
+
pRW50 + pTA100
P abiEi + AbiEi
P rv2827c + Rv2827c

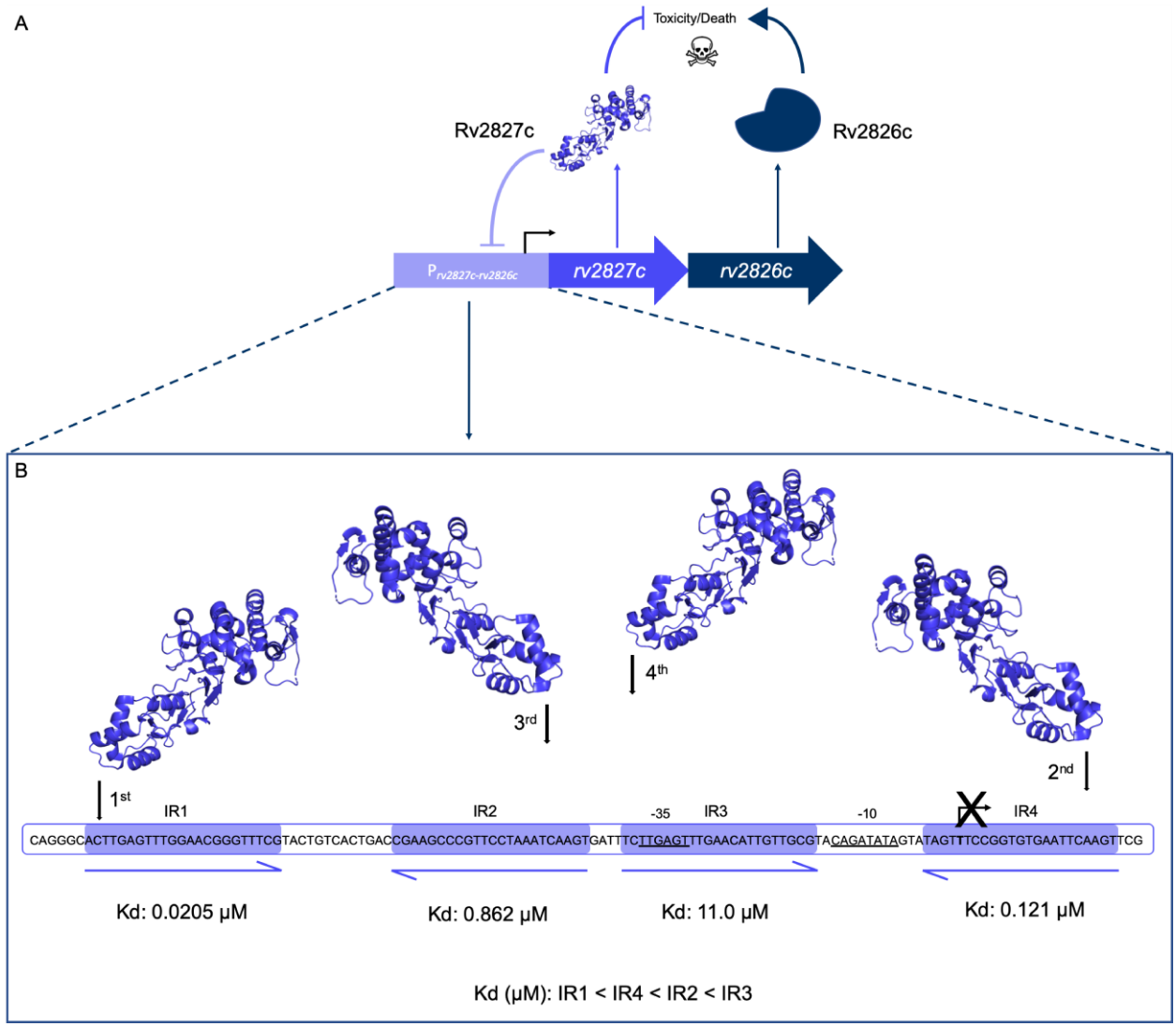
A
Toxicity/Death
Rv2827c
Rv2826c
P rv2827c-rv2826c
rv2827c
rv2826c
B
1st
3rd
4th
2nd
IR1
IR2
-35
IR3
-10
IR4
CAGGGCACTTGAGTTTGGAACGGGTTTCGTACTGTCACTGACCGAAGCCCGTTCCTAAATCAAGTGATTTCTTGAGTTTGAACATTGTTGCGTACAGATATAGTATAGTTTCCGGTGTGAATTCAAGTTCG
Kd: 0.0205 μM
Kd: 0.862 μM
Kd: 11.0 μM
Kd: 0.121 μM
Kd (μM): IR1 < IR4 < IR2 < IR3

SUPPLEMENTARY DATA

Antitoxin autoregulation of *M. tuberculosis* toxin-antitoxin expression through negative cooperativity arising from multiple inverted repeat sequences

Izaak N. Beck, Ben Usher, Hannah G. Hampton, Peter C. Fineran, Tim R. Blower*

SUPPLEMENTARY FIGURES

Fig. S1. AbiEi and Rv2827c have similar folds. Structure-based sequence alignment of AbiEi and Rv2827c, drawn by hand using output from PROMALS3D. Blue arrows represent β-sheets and pink ovals represent α-helices; numbers indicate amino acid positions.

Fig. S2. AbiEi binds with positive co-operativity to the IR1-IR2 region of the *abiE* promoter. (A) Sequence level cartoon of the fluorescently labelled probe containing IR1-IR2, with -35, -10, transcriptional start and ribosome binding site (RBS) indicated. (B) Electrophoretic mobility shift assay (EMSA) of titrated AbiEi with the probe in (A). (C) EMSA of titrated AbiEi with the probe in (A) altered by replacing IR2 with polyC. (D) EMSA of titrated AbiEi with the probe in (A) altered by replacing IR1 with polyC. (E) EMSA of titrated AbiEi with the probe in (A) altered by replacing both IR1 and IR2 with polyC. For (B-E); protein concentrations are shown on each panel together with the binding events (0, 1 or 2); S – each experiment contained 100-fold excess of the specific unlabelled probe; NS – each experiment contained 100-fold excess of non-specific unlabelled probe; numbering -1 to -71 denotes the promoter region included in the probe, upstream of the translational start site in order to include all of IR2. (F) Fractional saturation curve plotted using the EMSA data of (B). (G) Hill plot using the EMSA data from (B). For (F) and (G), points are plotted from triplicate data and display mean values with standard error of the mean.

Fig. S3. AbiEi and Rv2827c do not bind non-cognate promoters. (A) Electrophoretic mobility shift assay (EMSA) of titrated AbiEi with *rv2827c-rv2826c* promoter -1 to -71. (B) EMSA of titrated AbiEi with *rv2827c-rv2826c* promoter -61 to -131. (C) EMSA of titrated Rv2827c with *abiE* promoter -1 to -71. For (A-C); protein concentrations are shown below (C) together with the binding events (0, 1 or 2); S – each experiment contained 100-fold excess of the specific unlabelled probe; NS – each experiment contained 100-fold excess of non-specific unlabelled probe; numbering denotes the promoter region included in the probe, upstream of the translational start site in order to include all of the respective IR sequences.

Fig. S4. Rv1044 does not bind the cognate promoter but is capable of DNA-binding. (A) EMSA of titrated Rv1044 with *rv1044-rv1045* promoter -1 to -71. (B) EMSA of titrated Rv1044 with *rv1044-rv1045* promoter -61 to -131. (C) EMSA of titrated Rv1044 with *rv2827c-rv2826c* promoter -1 to -71. (D) EMSA of titrated Rv1044 with *rv2827c-rv2826c* promoter -61 to -131. (E) EMSA of titrated Rv1044 with *abiE* promoter -1 to -71. For (A-E); protein concentrations are shown on each panel together with the binding events (0, 1 or 2); S – each experiment contained 100-fold excess of the specific unlabelled probe; NS – each experiment contained 100-fold excess of non-specific unlabelled probe; numbering denotes the promoter region included in the probe, upstream of the translational start site in order to include all of the respective IR sequences. (F) Fractional saturation curve plotted using the EMSA data of (E). (G) Hill plot using the EMSA data from (E). For (F) and (G), points are plotted from triplicate data and display mean values with standard error of the mean.

60 # SUPPLEMENTARY TABLES

*Table S1. Oligonucleotides used in this study

Primer	Sequence[a]	Notes (Organism/Gene)
pRW50 cloning		
TRB1072	TTTGAATTCGATTTTGTTATCACAATAAATTGAGG	FWD EcoRI, 99 bp upstream of *abiEi*, *S. agalactiae*
TRB1047	TTTAAGCTTTACGGCCCCCCACTTGTTGC	REV HindIII, 99 bp upstream of *abiEi*, *S. agalactiae*
TRB1042	TTTGAATTCGCCCAAGCATCGGCTGGC	FWD EcoRI, 500 bp upstream of *rv2827c*, *M. tuberculosis*
TRB1043	TTTAAGCTTCCGAACTTGAATTCACACCGG	REV HindIII, 500 bp upstream of *rv2827c*, *M. tuberculosis*
TRB1040	TTTGAATTCGGGTCCCAACCGAGCGGC	FWD EcoRI, 500 bp upstream of *rv1044*, *M. tuberculosis*
TRB1041	TTTAAGCTTATTAGGTGATGGAGGCCAAGGCC	REV HindIII, 500 bp upstream of *rv1044*, *M. tuberculosis*
pSAT1-LIC cloning		
TRB873	TTAATGCAGCTGATTAATACG	FWD pSAT LIC sequencing
TRB875	TACTCAAGCTTATGCATGC	REV pSAT LIC sequencing
TRB1048	CAACAGCAGACGGGAGGTTCAAAAAAAGAGATTCTACTCGATTTTATAG	FWD *abiEi* LIC, *S. agalactiae*
TRB1049	GCGAGAACCAAGGAAAGGTTATTATATTAGAACCTCCAGAGTTTGTTTAAC	REV *abiEi* LIC, *S. agalactiae*
TRB1022	CAACAGCAGACGGGAGGTGTGAGCCCAGCCGGCGCC	FWD *rv2827c* LIC, *M. tuberculosis*
TRB1023	GCGAGAACCAAGGAAAGGTTATTACGCCTTGCCGATCACGCGCAGC	REV *rv2827c* LIC, *M. tuberculosis*
TRB1018	CAACAGCAGACGGGAGGTTGTGCAAAACCGTATCTAATTGATACGATTGCGC	FWD *rv1044* LIC, *M. tuberculosis*
TRB1019	GCGAGAACCAAGGAAAGGTTATTACGCCGATGCTCGCTTCGG	REV *rv1044* LIC, *M. tuberculosis*

pTA100 cloning

TRB1052	TTTGAATTCAGGAGGACAGGGATGTCAAAAAA AGAGATTCTACTC	FWD EcoRI, *abiEi*, *S. agalactiae*
TRB1053	TTTAAGCTTGGTTATTATATTAGAACCTCCAGA GTTTG	REV HindIII, *abiEi*, *S. agalactiae*
PF1334	TTTCATATGCAATTGAGGAGGACAGGGATGGT GAGCCCAGCCG	FWD NdeI/MfeI, *rv2827c, M. tuberculosis*
PF1335	TTTACTAGTCCCGGGGTCACGCCTTGCCGATC	REV SpeI/XmaI, *rv2827c, M. tuberculosis*
PF1330	TTTCATATGCAATTGAGGAGGACAGGGATGTG TGCAAAACCGTATCTAA	FWD NdeI/MfeI, *rv1044, M. tuberculosis*
PF1331	TTTACTAGTCCCGGGCTTGGTCACGCCGATG	REV SpeI/XmaI, *rv1044, M. tuberculosis*

EMSA probe primers and templates

TRB1067	TGCGCACTGACAAAAGCTT	REV EMSA untagged
TRB1068	/56-FAM/TGCGCACTGACAAAAGCTT	REV EMSA 56-FAM (fluorescein) tagged
TRB1061	AAAAGAAAATGTTGCTTTTATACCACAAATATT GTAAAATTGTAGTGTAAAAGCAACAAGTGGGG GGCCGTAAGCTTTTGTCAGTGCGCA	*S. agalactiae / abiEi -1 to -71* WT (**Fig. S2B**, **Fig. S3C**, **Fig. S4E**)
TRB1065	AAAAGAAAATGTTGCTTTTATACCACA	FWD for TRB1061, TRB1063, *S. agalactiae, abiEi*
TRB1062	AAAAGAAAACCCCCCCCCCCTACCACAAATATT GTAAAATTGTAGTGTAAAAGCAACAAGTGGGG GGCCGTAAGCTTTTGTCAGTGCGCA	*S. agalactiae / abiEi -1 to -71* Mutant; inverted repeat 1 poly-C track substitution (**Fig. S2D**)
TRB1066	AAAAGAAAACCCCCCCCC	FWD for TRB1062, TRB1064, *S. agalactiae, abiEi*
TRB1063	AAAAGAAAATGTTGCTTTTATACCACAAATATT GTAAAATTGTAGTGCCCCCCCCCCCAGTGGGG GGCCGTAAGCTTTTGTCAGTGCGCA	*S. agalactiae / abiEi -1 to -71* Mutant; inverted repeat 2 poly-C track substitution (**Fig. S2C**)
TRB1064	AAAAGAAAACCCCCCCCCCCTACCACAAATATT GTAAAATTGTAGTGCCCCCCCCCCCAGTGGGG GGCCGTAAGCTTTTGTCAGTGCGCA	*S. agalactiae / abiEi -1 to -71* Mutant; inverted repeat 1 & 2 poly-C track substitution (**Fig. S2E**)

TRB1086	AACTAGGCGCGCCTAGCCTGGACGAGTCCCCG GGCCGACATTCGCCCGAGGCCTTGGCCTCCAT CACCTAAAAGCTTTTGTCAGTGCGCA	*M. tuberculosis* H37Rv */ rv1044, -1 to -71* WT (**Fig. S4A**)
TRB1087	AACTAGGCGCGCCTAG	FWD for TRB1086, *M. tuberculosis, rv1044*
TRB1102	GTATCTGCGACAAGGGCAGCGTCGATGCCTCG ACATGCAGAGTCGGTGTTCGCTTCACGCGAAC TAGGCGCAAGCTTTTGTCAGTGCGCA	*M. tuberculosis* H37Rv */ rv1044, -61 to -131* WT (**Fig. S4B**)
TRB1103	GTATCTGCGACAAGGGCAG	FWD for TRB1102, *M. tuberculosis, rv1044*
TRB1104	CAAGTGATTTCTTGAGTTTGAACATTGTTGCGT ACAGATATAGTATAGTTTCCGGTGTGAATTCAA GTTCGAAGCTTTTGTCAGTGCGCA	*M. tuberculosis* H37Rv */ rv2827c, -1 to -71* WT (**Fig. 4B**, **Fig. S3A, Fig. S4C**)
TRB1105	CAAGTGATTTCTTGAGTTTGAACATTG	FWD for TRB1104, TRB1271, *M. tuberculosis, rv2827c*
TRB1106	CAGGGCACTTGAGTTTGGAACGGGTTTCGTAC TGTCACTGACCGAAGCCCGTTCCTAAATCAAGT GATTTCAAGCTTTTGTCAGTGCGCA	*M. tuberculosis* H37Rv */ rv2827c, -61 to -131* WT (**Fig. 5B, Fig. S3B, Fig. S4D**)
TRB1107	CAGGGCACTTGAGTTTGGAAC	FWD for TRB1106, TRB1277, full-length *-1 to -131* (**Fig. 6A**), *M. tuberculosis, rv2827c*
TRB1108	TGGCATTCAATCGATGGCTTCCTAGTTTTAGAT GATTAGGGCTTGTCCCAAATGGATTGAGAGGT TGACAAAGCTTTTGTCAGTGCGCA	Plasmid pEFER, 12851-12920 bp NS probe (**Fig. 4 – 6, Fig. S2 – S4**)
TRB1109	TGGCATTCAATCGATGGCTT	FWD plasmid pEFER NS probe
TRB1271	CAAGTGATTCCCCCCCCCCCCCCCCCCCCCCCTA CAGATATAGTATAGTTTCCGGTGTGAATTCAAG TTCGAAGCTTTTGTCAGTGCGCA	*M. tuberculosis* H37Rv */ rv2827c, -1 to -71* Mutant; inverted repeat 3 poly-C track substitution (**Fig. 4D**)
TRB1272	CAAGTGATTCCCCCCCCC	FWD for TRB1271, TRB1274, *M. tuberculosis, rv2827c*
TRB1273	CAAGTGATTTCTTGAGTTTGAACATTGTTGCGT ACAGATATAGTACCCCCCCCCCCCCCCCCCCCC CCTCGAAGCTTTTGTCAGTGCGCA	*M. tuberculosis* H37Rv */ rv2827c, -1 to -71* Mutant; inverted repeat 4 poly-C track substitution (**Fig. 4C**)
TRB1274	CAAGTGATTCCCCCCCCCCCCCCCCCCCCCCCTA CAGATATAGTACCCCCCCCCCCCCCCCCCCCC CTCGAAGCTTTTGTCAGTGCGCA	*M. tuberculosis* H37Rv */ rv2827c, -1 to -71* Mutant; inverted repeat 3 & 4 poly-C track substitution (**Fig. 4E**)

TRB1275	CAGGGCCCCCCCCCCCCCCCCCCCCCCCCTACT GTCACTGACCGAAGCCCGTTCCTAAATCAAGT GATTTAAGCTTTTGTCAGTGCGCA	*M. tuberculosis* H37Rv */ rv2827c, -61 to -131* Mutant; inverted repeat 1 poly-C track substitution (**Fig. 5D**)
TRB1276	CAGGGCCCCCCCCCC	FWD for TRB1275, TRB1278, *M. tuberculosis, rv2827c*
TRB1277	CAGGGCACTTGAGTTTGGAACGGGTTTCGTAC TGTCACTGACCCCCCCCCCCCCCCCCCCCCCCCC GATTTAAGCTTTTGTCAGTGCGCA	*M. tuberculosis* H37Rv */ rv2827c, -61 to -131* Mutant; inverted repeat 2 poly-C track substitution (**Fig. 5C**)
TRB1278	CAGGGCCCCCCCCCCCCCCCCCCCCCCCCTACT GTCACTGACCCCCCCCCCCCCCCCCCCCCCCCG ATTTAAGCTTTTGTCAGTGCGCA	*M. tuberculosis* H37Rv */ rv2827c, -61 to -131* Mutant; inverted repeat 1 & 2 poly-C track substitution (**Fig. 5E**)

[a]EMSA probe sequences are fused with a constant region from the *lacZ* gene of pRW50, highlighted in grey. The reverse primers (TRB1067 and TRB1069) anneal to this sequence for amplification.

Table S2. Plasmids used in this study

Plasmid	Construct	Cloning technique	Primer set/Restriction enzymes used	Reference
pPF656	pTA100-*rv1044*	Restriction Cloning	PF1330/PF1331	This work
pPF658	pTA100-*rv2827c*	Restriction Cloning	PF1334/PF1335	This work
pRLD30	pTRB30-His_6-*abiEi*	-	-	[15]
pRW50	Tc^R	-	-	[32]
pSAT1-LIC	Ap^R	-	-	This work
pTA100	Sm^R	-	-	[5]
pTRB481	pTA100-*abiEi*	Restriction Cloning	TRB1052/TRB1053	This work
pTRB483	pRW50-500 bp upstream *rv1044*	Restriction Cloning	TRB1040/TRB1041	This work
pTRB484	pRW50-500 bp upstream *rv2827c*	Restriction Cloning	TRB1042/TRB1043	This work
pTRB486	pRW50-99 bp upstream *abiEi*	Restriction Cloning	TRB1072/TRB1047	This work
pTRB491	pSAT1-LIC-*rv1044*	Ligation Independent Cloning	TRB1018/TRB1019	This work
pTRB493	pSAT1-LIC-*rv2827c*	Ligation Independent Cloning	TRB1022/TRB1023	This work
pTRB525	pSAT1-LIC-*abiEi*	Ligation Independent Cloning	TRB1048/TRB1049	This work

```
AbiEi:      2    -----------SKKEILLDFIEKNNG-IVTNKDCKALGIP-------TIYLTRLEKEGII    42
Rv2827c:    2    VSPAGADRRIPTWASRVVSGLARDRPVVVTKEDLTQRLTEAGCGRDPDSAIRELRRIG--    59
Consensus ss:

AbiEi:      43   FRVE-----KGIFLTQNG--DYDEYYFFQYRF------PKAIFSYISALYLQQFTDEIPQ    89
Rv2827c:    60   WLVQLPVKGTWAFIPPGEAAISDPY-LPLRSWLARDQNAGFMLAGASAAWHLGYLDRQPD    118
Consensus ss:

AbiEi:      90   Y-FDVTVPRG-YRFNTPPANLNIHFVSKEYS-E-LGMT------------TVPTPMGNNV    133
Rv2827c:    119  GRIPIWLPPAKRLPDGLASYVSVVRIPWNAADTALLAPRPALLVRRRLDLVAWA---TGL    175
Consensus ss:

AbiEi:      134  RVYDFERIICDFVIHREKIDSELFVKTLQSYGNYPKKNL-AKLYEYATKMN--TLEKVKQ    190
Rv2827c:    176  PALGPEALLVQIATRPASF-GPWADLVPHLDDLVADCSDERLERLLSGRPTSAWQRASYL    234
Consensus ss:

AbiEi:      191  TLEVLI-------------------------------------------------------    196
Rv2827c:    235  LDSGGEPARGQALLAKRHTEVMPVTRFTTAHSRDRGESVWAPEYQLVDELVVPLLRVIGKA    295
Consensus ss:
```

A

-35 IR1 -10 IR2 RBS

AAAAGAAAATGTTGCTTTTATACCACAAATATTGTAAAATTGTAGTGTAAAAGCAACAAGTGGGGGGCCGT

[AbiEi]

S NS

B

abiEi -1 to -71

IR1 – IR2

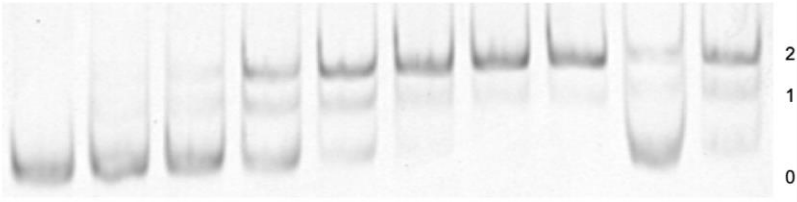

Protein (μM) 0 0.025 0.075 0.2 0.5 1.0 2.0 5.0 0.5 0.5

C

abiEi -1 to -71

IR1 – ~~IR2~~

Protein (μM) 0 0.0078 0.015 0.03 0.0625 0.125 0.25 0.5 0.25 0.25

D

abiEi -1 to -71

~~IR1~~ – IR2

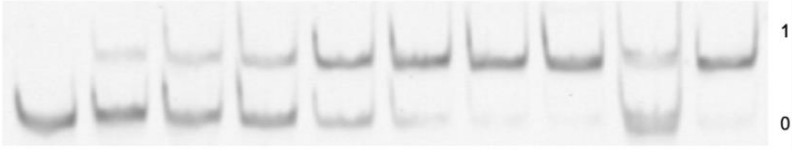

Protein (μM) 0 0.0125 0.025 0.05 0.075 0.2 0.5 2.0 0.075 0.075

E

abiEi -1 to -71

~~IR1~~ – ~~IR2~~

Protein (μM) 0 0.025 0.075 0.2 0.5 1.0 2.0 5.0 0.5 0.5

F

abiEi -1 to -71

Saturation curve

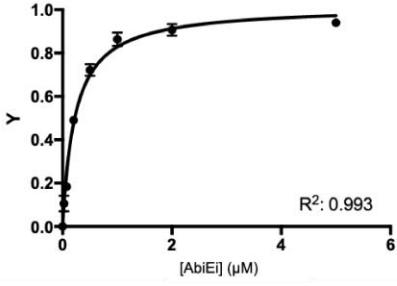

G

abiEi -1 to -71

Hill plot

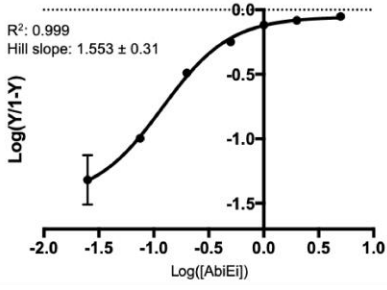

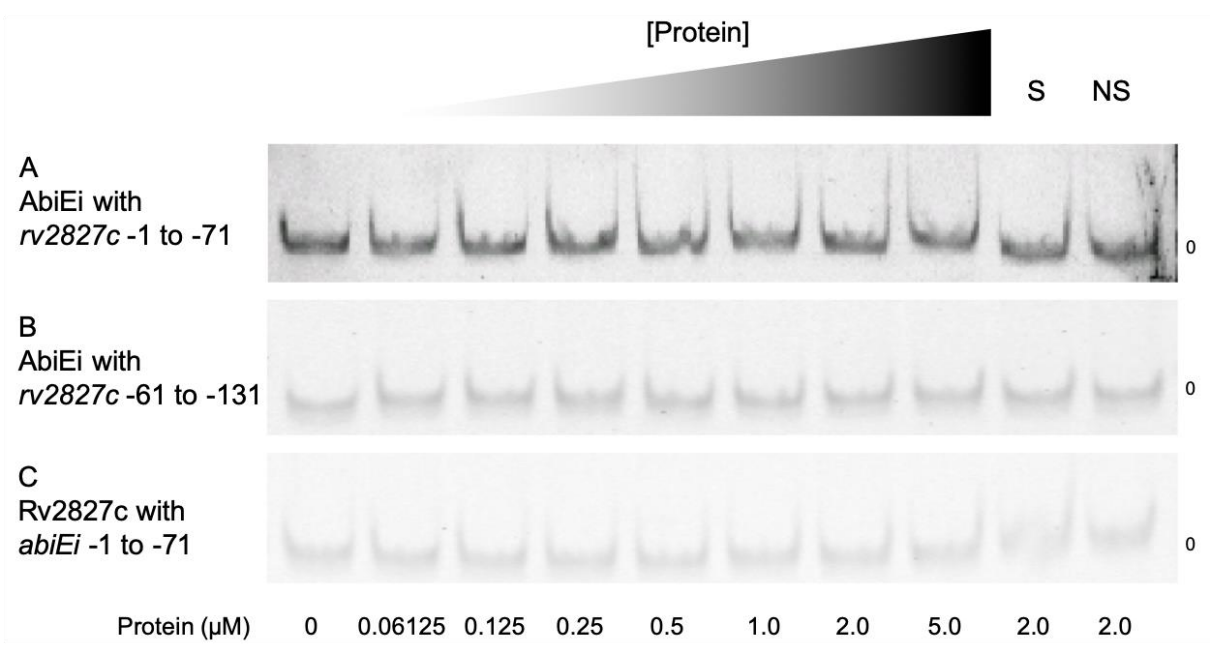
[Protein]
S
NS
A
AbiEi with
rv2827c -1 to -71
0
B
AbiEi with
rv2827c -61 to -131
0
C
Rv2827c with
abiEi -1 to -71
0
Protein (μM)
0
0.06125
0.125
0.25
0.5
1.0
2.0
5.0
2.0
2.0

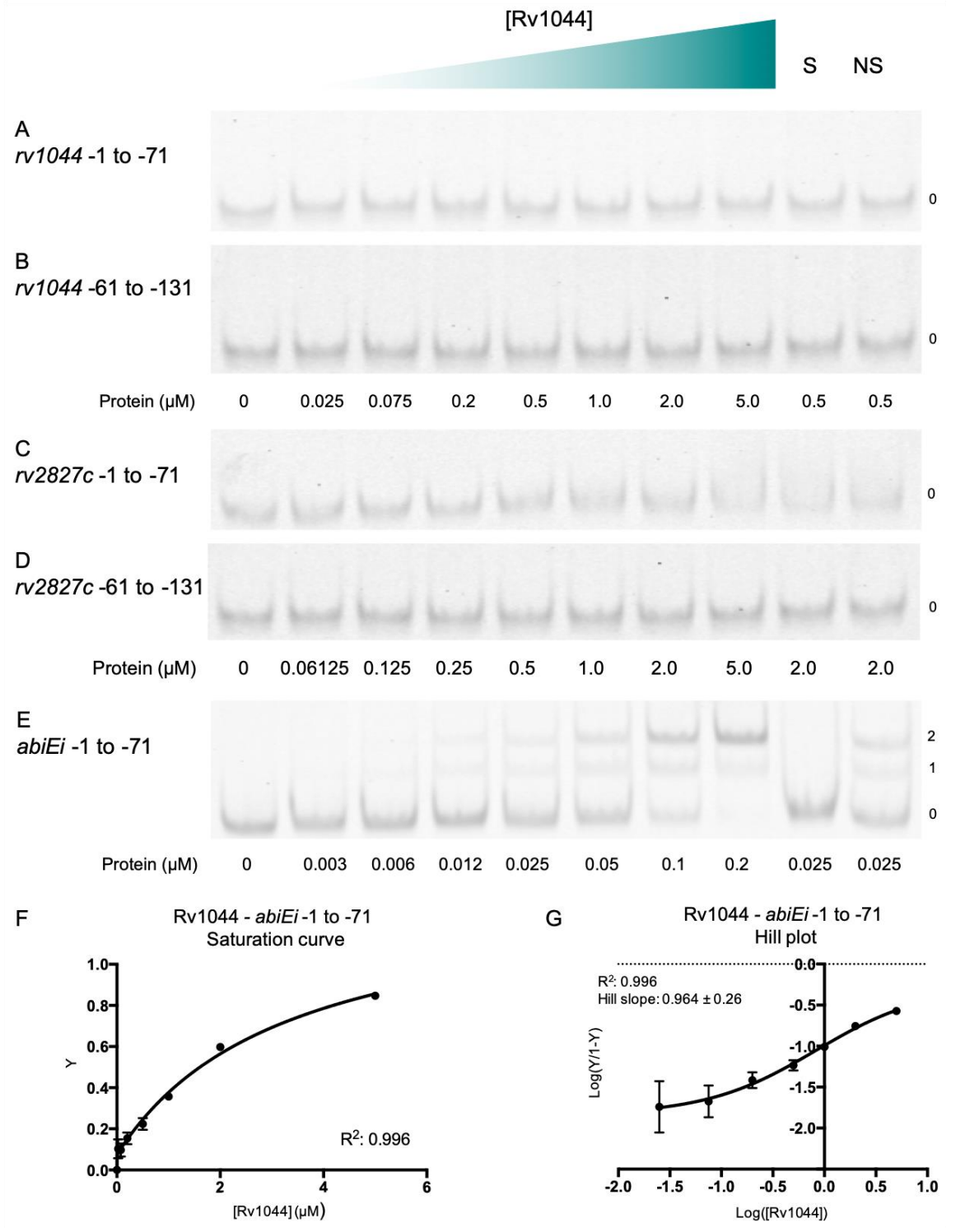
[Rv1044]
S
NS
A
rv1044 -1 to -71
0
B
rv1044 -61 to -131
0
Protein (μM) 0 0.025 0.075 0.2 0.5 1.0 2.0 5.0 0.5 0.5
C
rv2827c -1 to -71
0
D
rv2827c -61 to -131
0
Protein (μM) 0 0.06125 0.125 0.25 0.5 1.0 2.0 5.0 2.0 2.0
E
abiEi -1 to -71
2
1
0
Protein (μM) 0 0.003 0.006 0.012 0.025 0.05 0.1 0.2 0.025 0.025
F
Rv1044 - abiEi -1 to -71
Saturation curve
Y
1.0
0.8
0.6
0.4
0.2
0.0
0
2
4
6
[Rv1044] (μM)
R2: 0.996
G
Rv1044 - abiEi -1 to -71
Hill plot
R2: 0.996
Hill slope: 0.964 ± 0.26
Log(Y/1-Y)
0.0
-0.5
-1.0
-1.5
-2.0
-2.0
-1.5
-1.0
-0.5
0.0
0.5
1.0
Log([Rv1044])